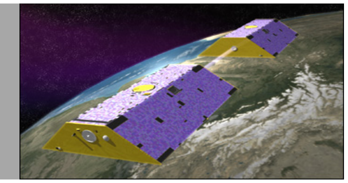

Coseismic Earthquake Deformation Modeling Using Spaceborne Geodetic Sensors

王雷 (Lei Wang)

2011 Summer School

Shanghai Astronomical Observatory, Chinese Academy of Sciences

July 17~July 21, 2011

School of Earth Science,

Division of Geodetic Science,

Ohio State University, USA

Outline

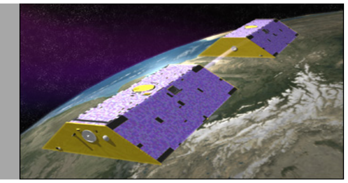

- General introduction of earthquakes and their physical mechanism
- Dislocation theory and practical computations
- Seismic data and Geodetic sensors capable of measuring earthquake coseismic deformation
- GRACE and Slepian function localization
- Examples of the great earthquakes detection and inversion by InSAR, GPS, GRACE

Earthquakes And Their Physical Mechanism

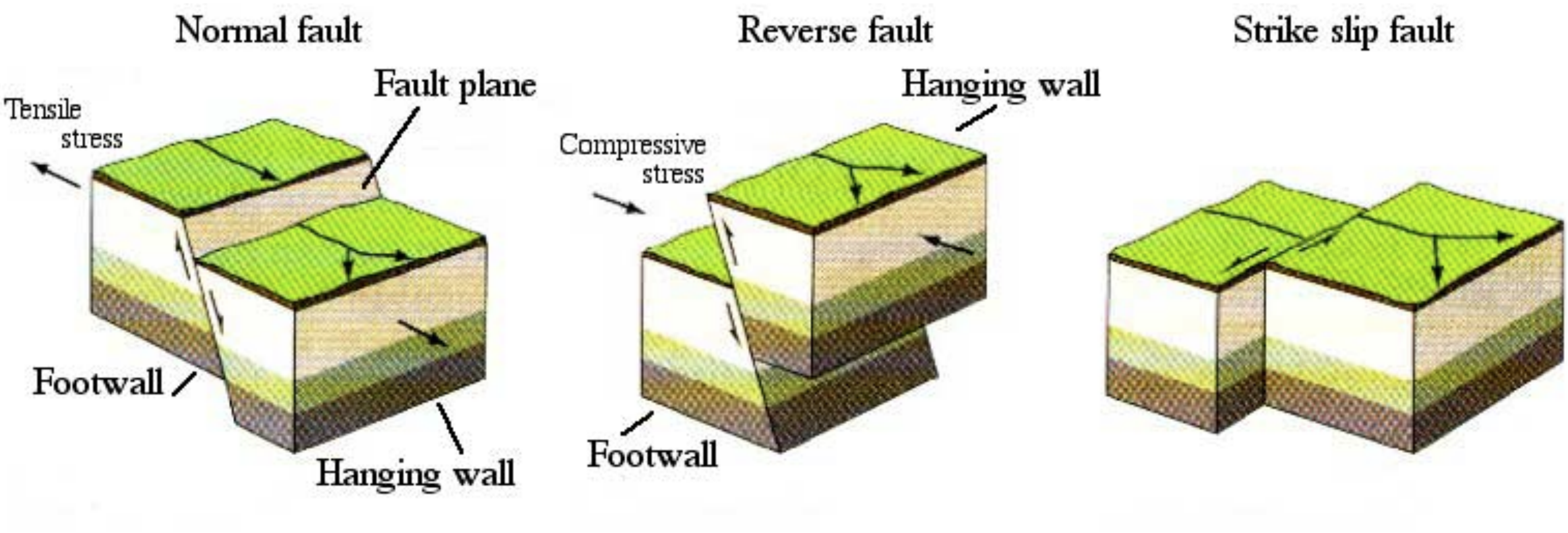

Faults are fractures in the crust, usually found along plate boundaries.

The three different stresses upon the crust result in fractures of three different types:
a) tension stress - normal fault - hanging wall slides down/footwall slides up
b) compression stress - reverse fault - hanging wall slides up/footwall slides down
c) torsion (twist) stress - strike slip fault - ground moves past itself

THE OHIO STATE UNIVERSITY

Earthquakes And Their Physical Mechanism

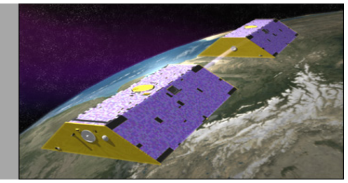

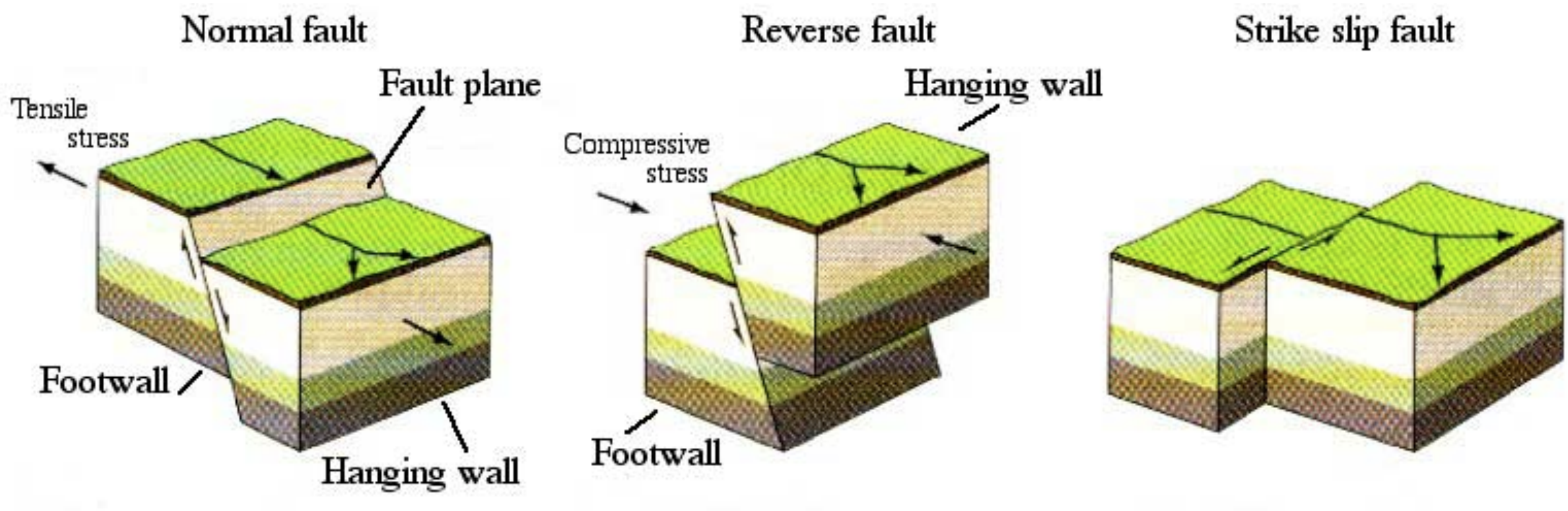

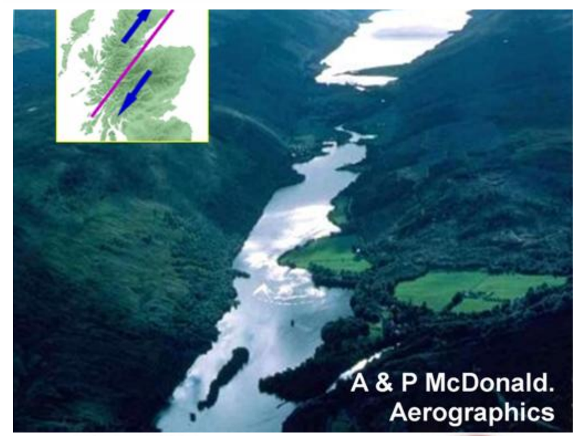

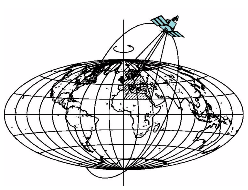

School of Earth Sciences

Faulting parameters

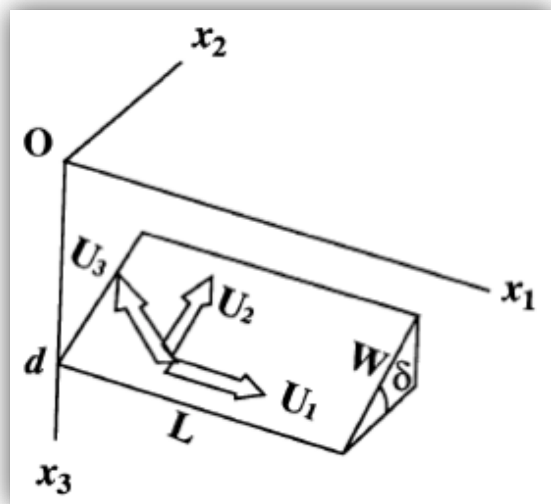

Coseismic deformation

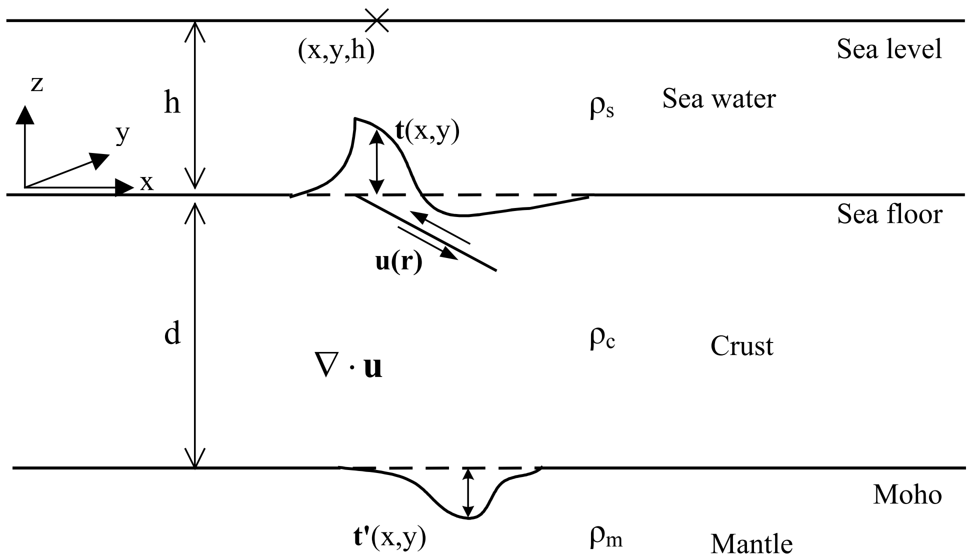

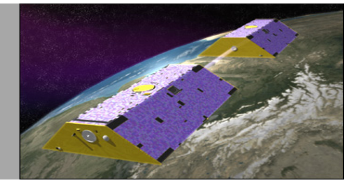

Coseismic Deformation Modeling

1. Okada [1992]

Modeling internal/surface deformation due to shear and tensile faults in a homogeneous half-space.

2. Rongjiang Wang

M

gr

di

3.

D

to internal dislocations in a spherical, layered earth.

Interesting studies:

1. Half-space vs. Spherical model
2. Homogeneous vs. layered model
3. Dislocation theory vs. Normal mode

4. Pollitz [1996]

Coseismic deformation from earthquake faulting on a layered spherical earth.

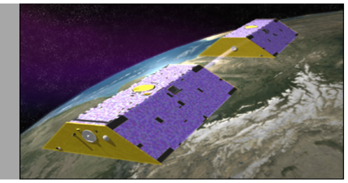

Coseismic gravity/gravity gradients changes modeling

(1) perturbation to the density field . Here is the dislocation vector of each integral point on the fault plane.
(2) the surface mass density that accompanies the uplift/subsidence of the ground.
(3)attraction of matter with density that intrude into the cavity by tensile fracturing.

$$\Delta\psi(\mathbf{r};\xi_3) = \rho G \int_V \frac{\nabla\cdot\mathbf{u}(\mathbf{r}')}{|\mathbf{r}-\mathbf{r}'|} dV' - \rho' G \frac{1}{|\mathbf{r}-\mathbf{r}'|} \Delta u_i n_i \, d\Sigma$$

1. Analytical method. ➔ Green's function
2. Numerical method.

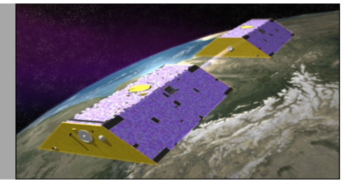

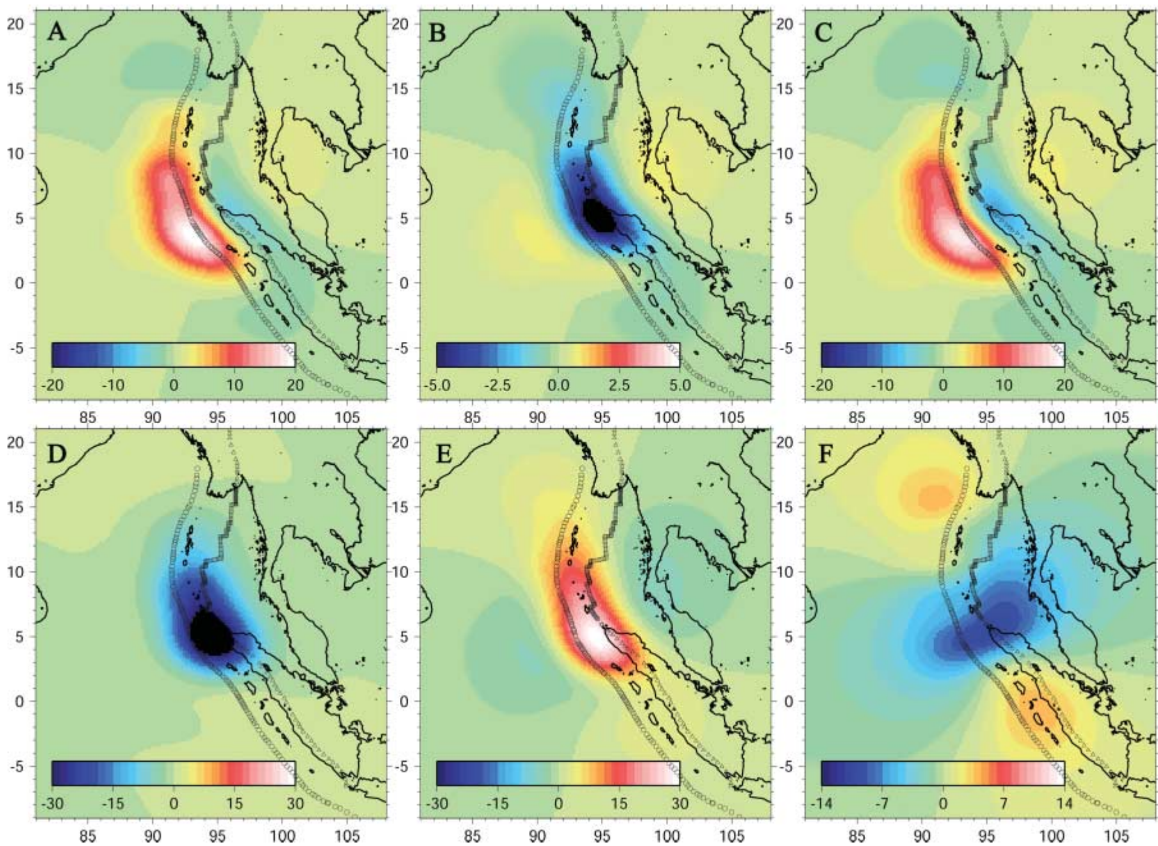

Coseismic gravity changes due to uplift/subsidence

Coseismic gravity changes due to dilatation (internal density changes)

[Han et al., 2006, Science]

Coseismic gravity gradients changes due to uplift/subsidence

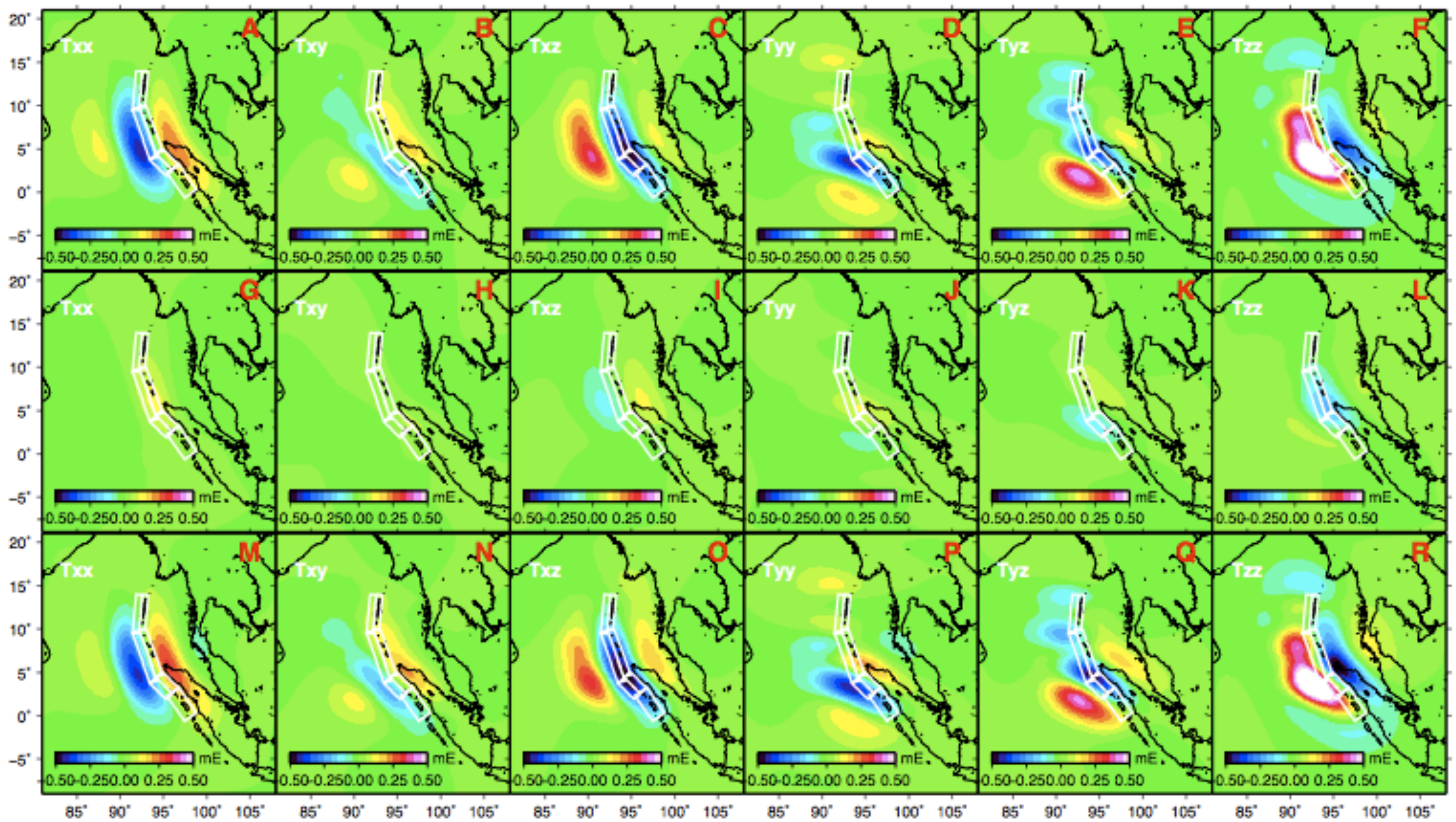

Coseismic gravity gradients changes due to dilatation

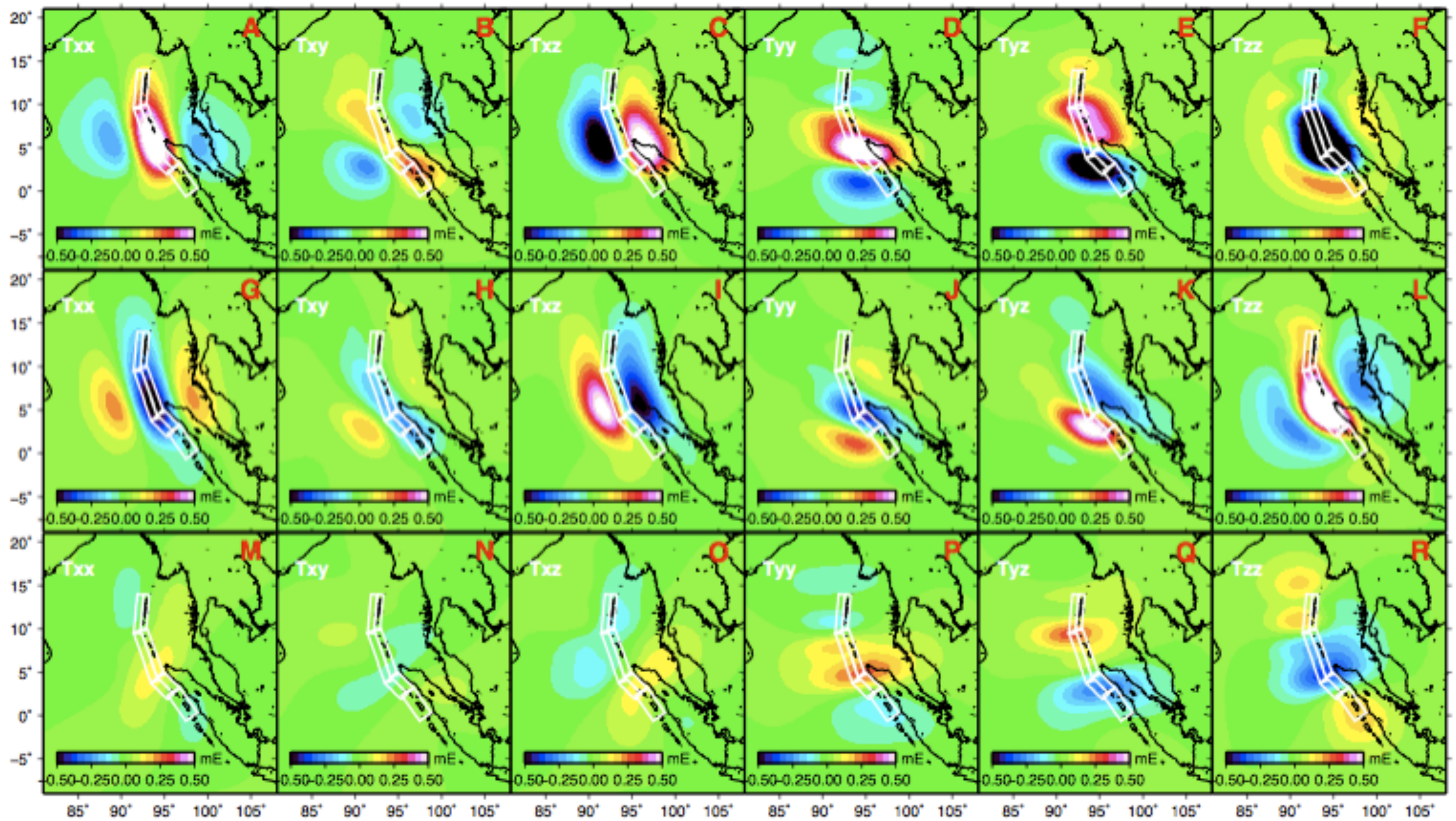

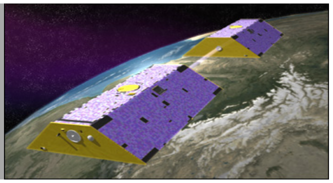

GPS (Global Positioning Systme)

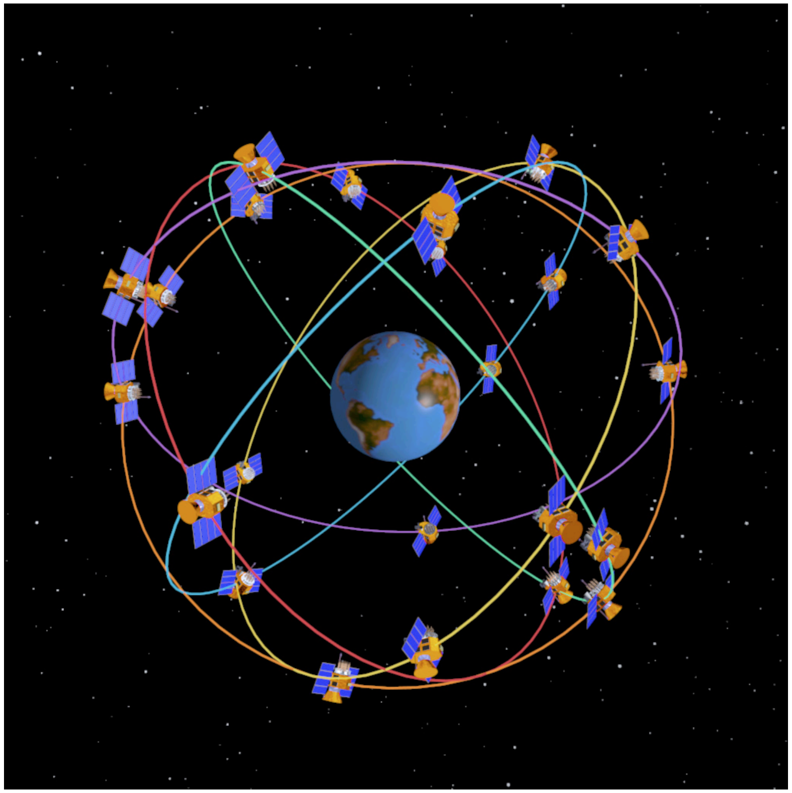

School of Earth Sciences

AIRA Preliminary Coseismic Displacements from March 11, 2011 Sendai-Oki Earthquake

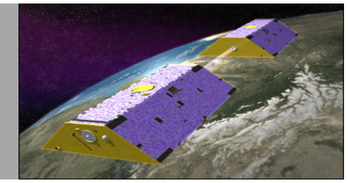

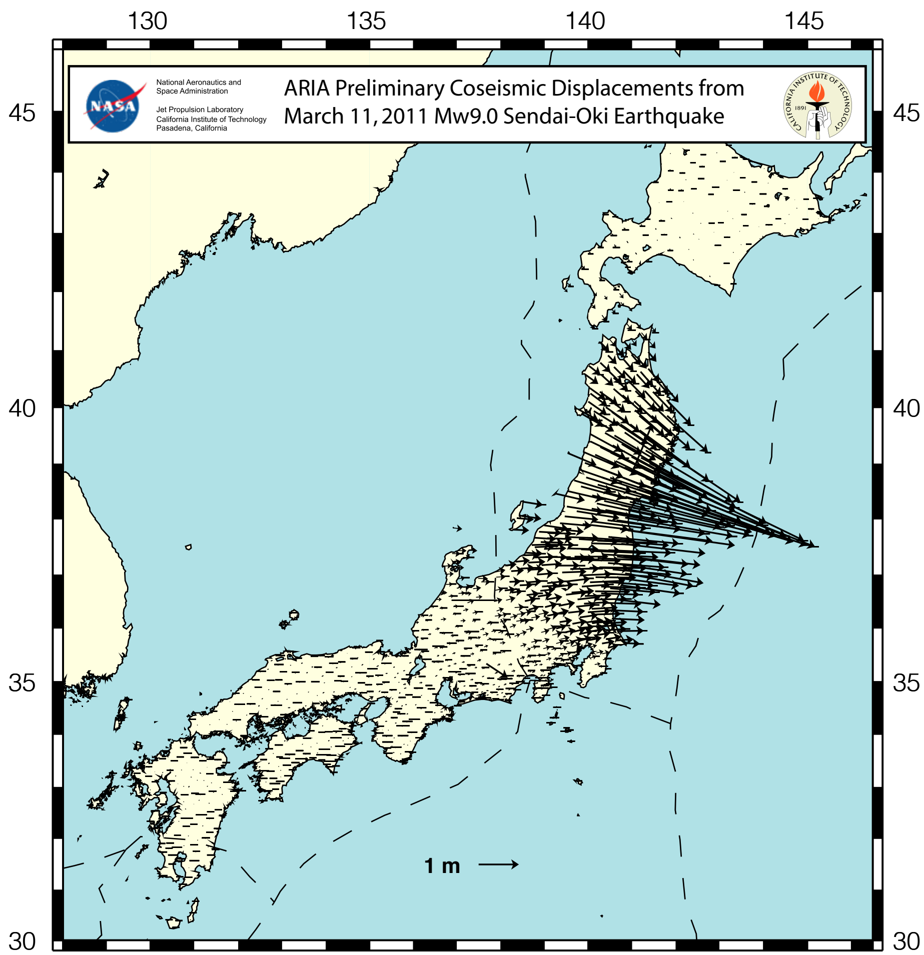

Figure shows version 0.2 horizontal displacements based on difference between estimated positions of GEONET stations at 05:00 and 06:30 UTC on March 11, using JPL's Rapid orbit solution and using JPL's GIPSY-OASIS software. Bars at end of vector show 95% error estimate. Solutions courtesy of ARIA team at JPL and Caltech. All original GEONET RINEX data provided to Caltech by the Geospatial Information Authority (GSI) of Japan.

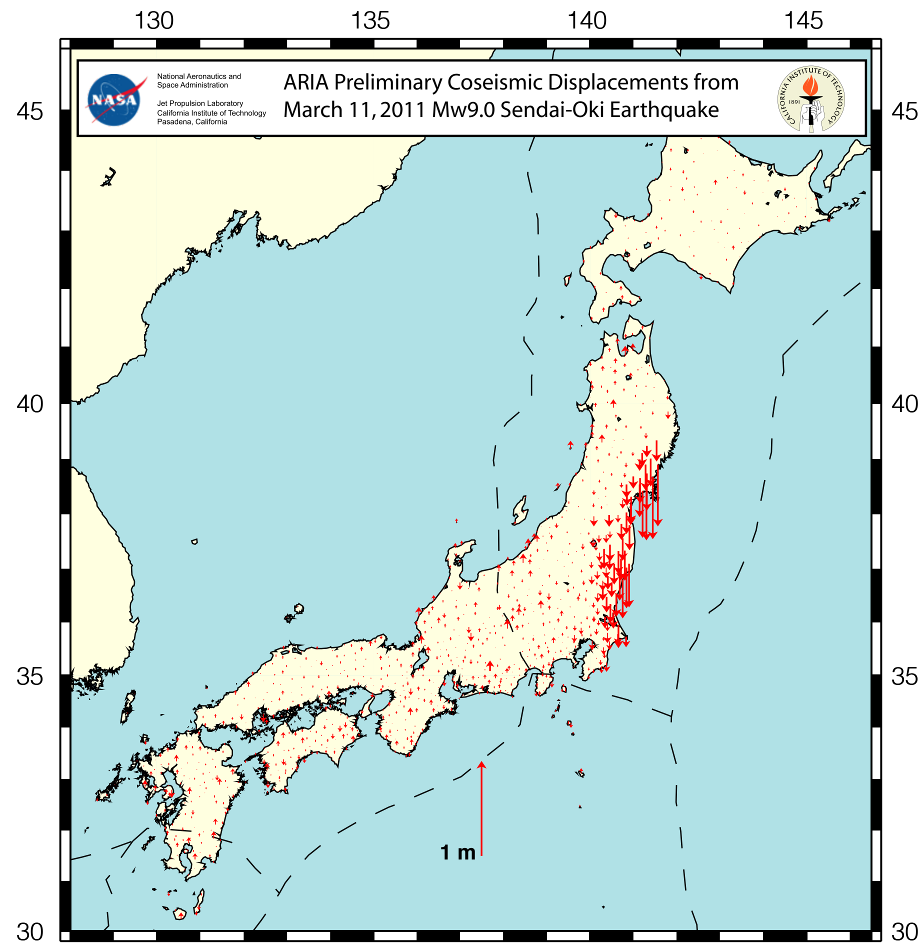

Figure shows version 0.2 vertical displacements based on difference between estimated positions of GEONET stations at 05:00 and 06:30 UTC on March 11, using JPL's Rapid orbit solution and using JPL's GIPSY-OASIS software. Solutions courtesy of ARIA team at JPL and Caltech. All original GEONET RINEX data provided to Caltech by the Geospatial Information Authority (GSI) of Japan.

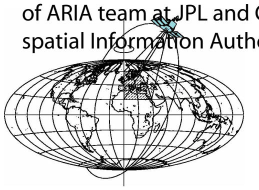

School of Earth Sciences

Geodetic Sensors Capable of Measuring Coseismic Deformation

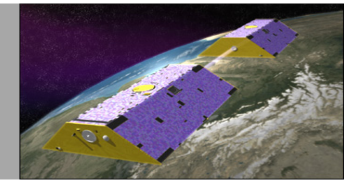

Synthetic Aperture Radar (SAR)
- Microwave imaging system (cm to dm wavelength)
- Cloud penetrating capability
- Active system -- Day and night operational capability

Interferometric SAR or 'InSAR': exploits the phase difference of at least two Complex-valued SAR images acquired from different orbit positions and/or at different times. Accurately measure the radiation travel path. Measurements of travel path variations as a function of the satellite position and time of acquisition allow generation of Digital Elevation Models (DEM) and measurement of centimetric surface deformations of the terrain.

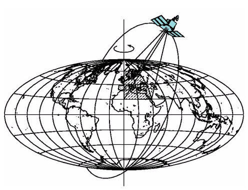

Geodetic Sensors Capable of Measuring Coseismic Deformation

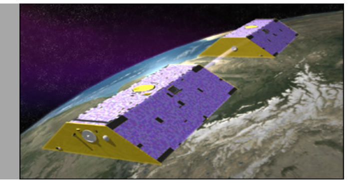

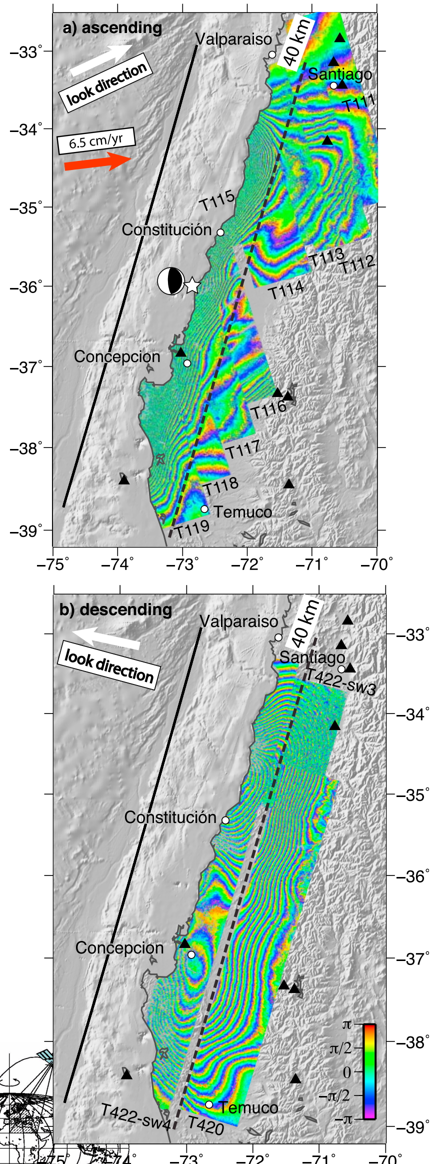

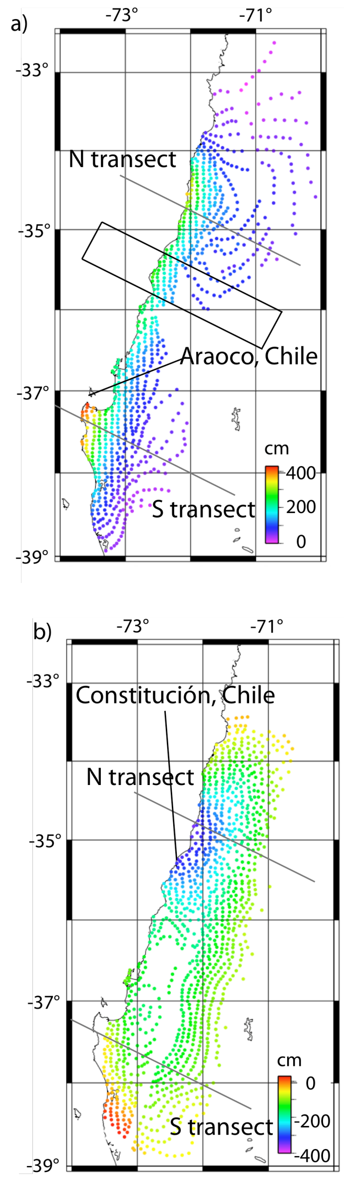

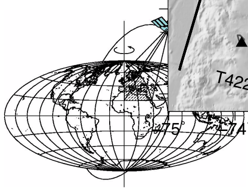

Ascending tracks

Descending tracks

Radar interferometry from the ALOS satellite caputred the coseismic ground deformation associated with the 2010 Mw 8.8 Maule, Chile earthquake.

[Tong et al., GRL 2010]

Geodetic Sensors Capable of Measuring Coseismic Deformation

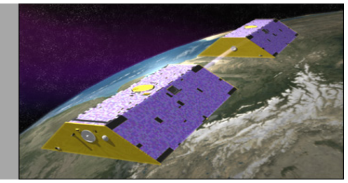

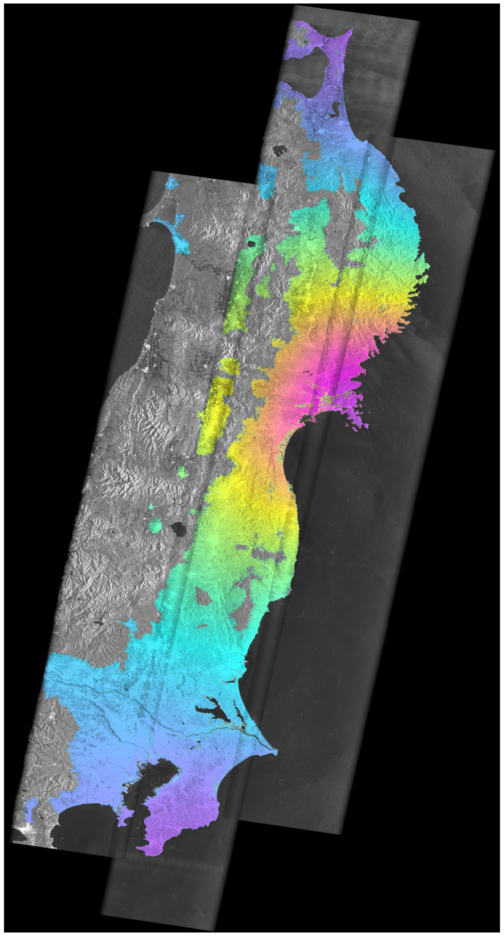

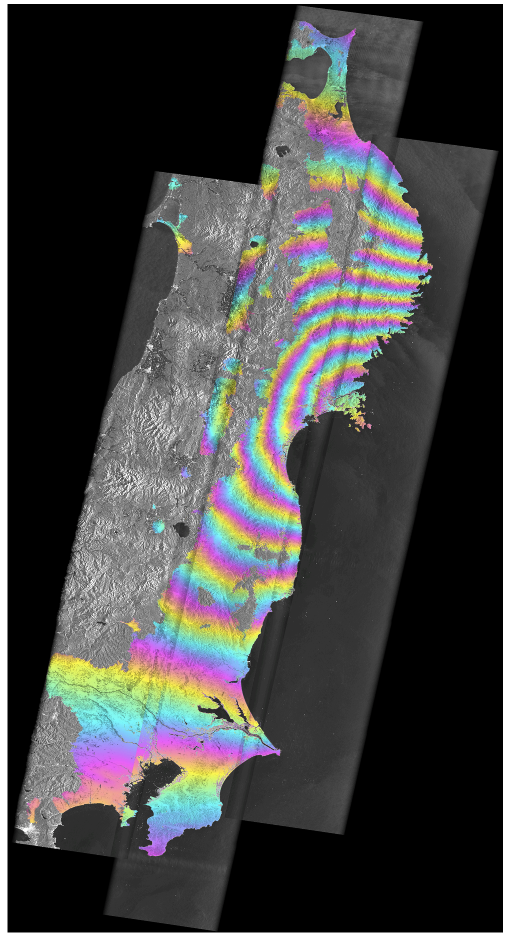

ENVISAT Asar：

wavelength: 5.6 cm
incidence angle: 40.6520°
width: 4695, lines: 8784
heading: -170.0188370°

Three tracks:
2011. 02. 19 ~ 2011. 03. 21,
2011. 03. 02 ~ 2011. 04. 01,
2011. 02. 08 ~2011. 04. 09

March 11, 2011
Sendai-Oki Earthquake

Geodetic Sensors Capable of Measuring Coseismic Deformation

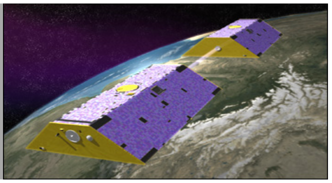

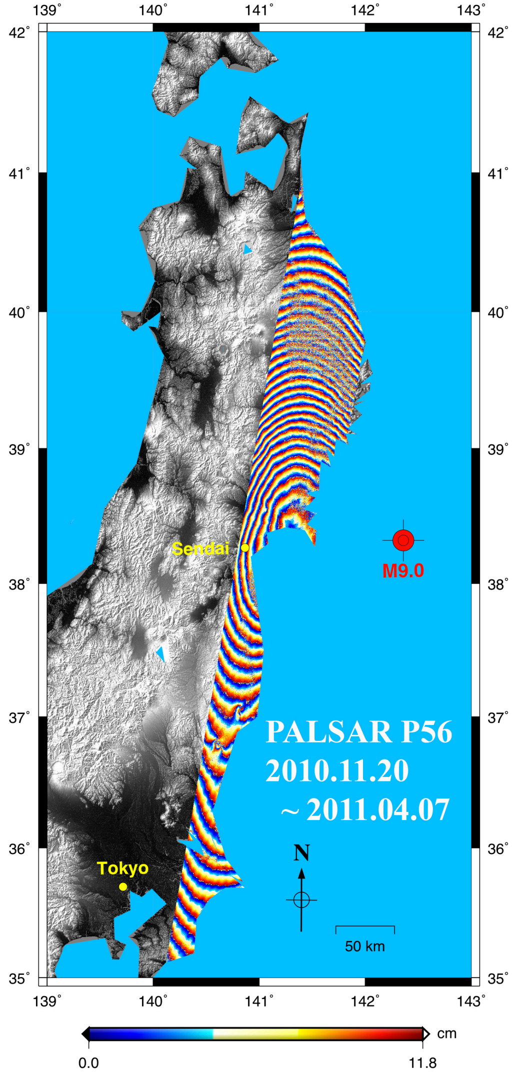

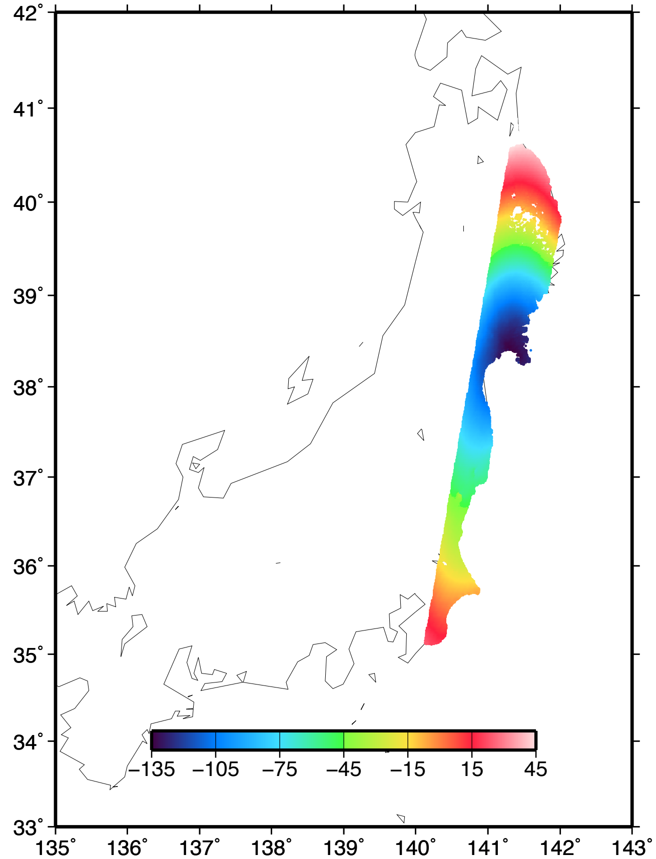

Alos Palsar:

wavelength: 23.6 cm
incidence angle: 38.79°
heading: -169.994412°

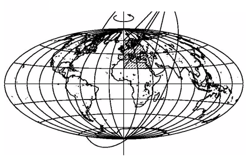

March 11, 2011
Sendai-Oki Earthquake

School of Earth Sciences

Geodetic Sensors Capable of Measuring Coseismic Deformation

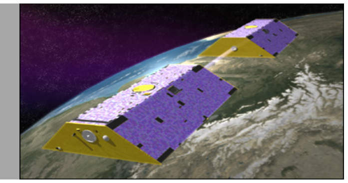

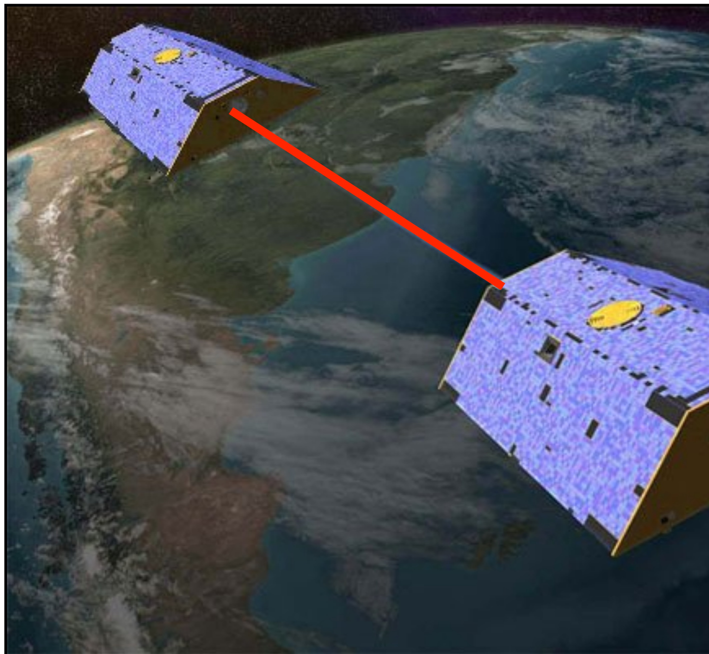

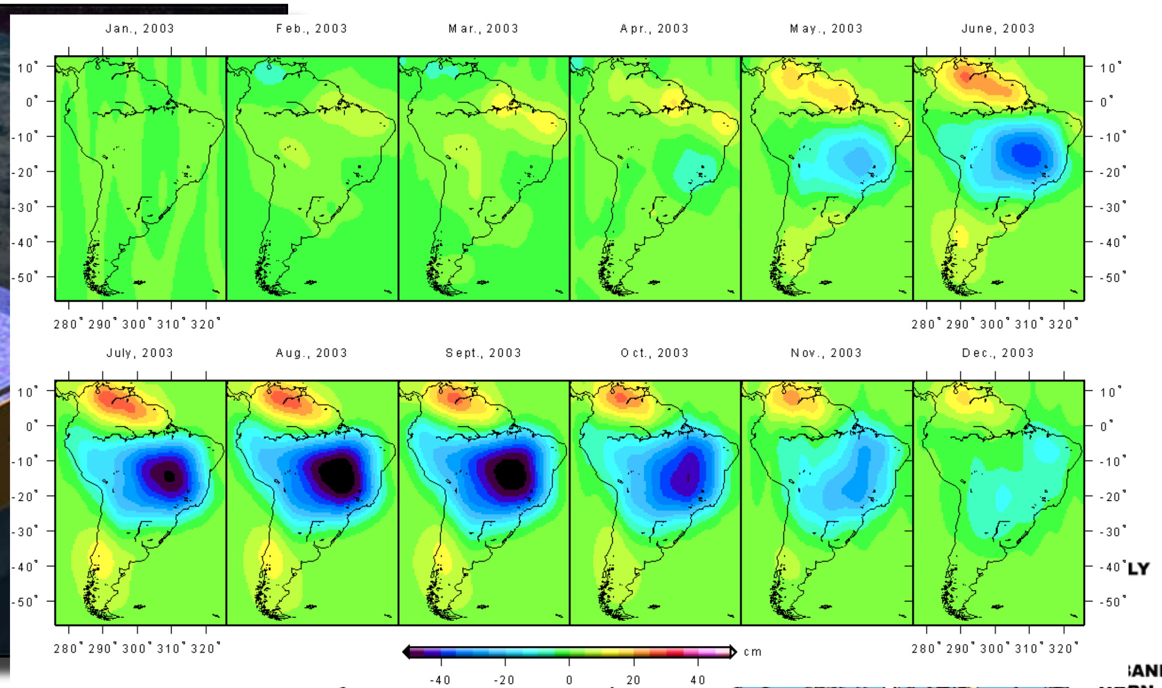

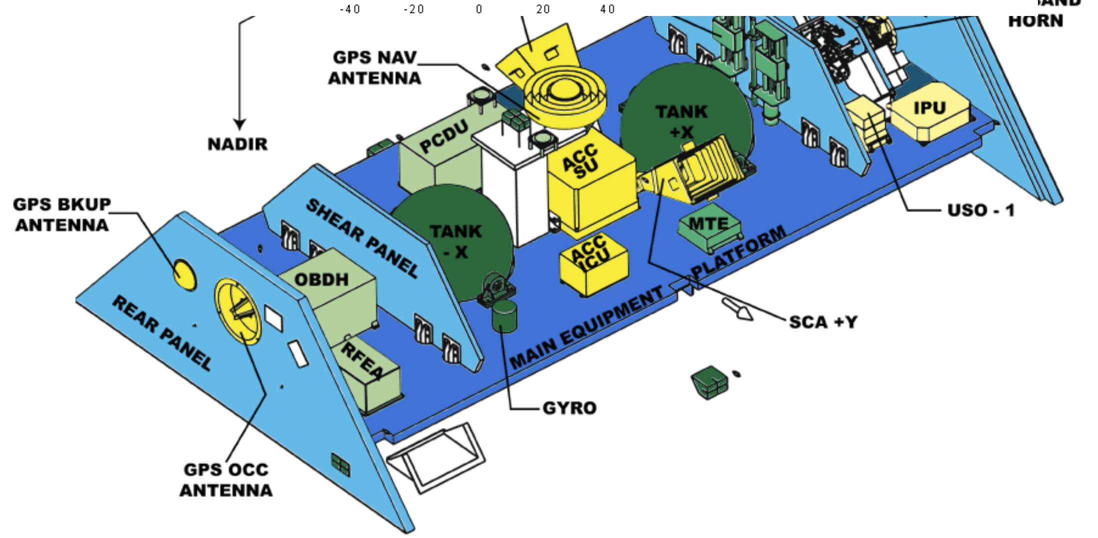

GRACE:

- Launch: March 2002
- Altitude: 470 km
- Separation distance: 220 km
- Inclination: 89^0
- KBR Precision ~ 1 μm

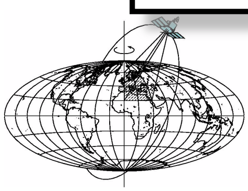

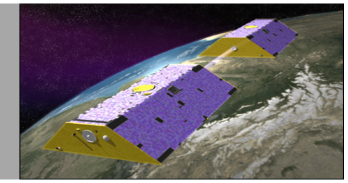

Coseismic deformation from GRACE
I. Regional solution

KBR range-rate

Frictional energy (accelerometer/star camera)

From GPS

$$\tilde{\dot{\rho}}_{12} = \frac{1}{|\dot{\mathbf{x}}_1|} V_{12} + \frac{1}{|\dot{\mathbf{x}}_1|} E^F_{12} + \frac{1}{|\dot{\mathbf{x}}_1|} E^R_{12} - \frac{1}{|\dot{\mathbf{x}}_1|} \dot{\mathbf{x}}_1 \cdot \dot{\mathbf{x}}_{12} - \frac{1}{2|\dot{\mathbf{x}}_1|} \dot{\mathbf{x}}_{12} \cdot \dot{\mathbf{x}}_{12} + \mathbf{e}_{12} \cdot \dot{\mathbf{x}}_{12} + \text{const} + \varepsilon$$

In situ disturbance potential

Rotational energy (GPS)

- Jekeli (1999) and Han et al. (2005)
- GRACE L1B data and precise orbit used.

δV_{12} (relative to GGM01C) is estimated with inter-satellite orbit and other parameters (KBR & accelerometer biases)

- 0.008 m^2/s^2 $\delta V_{12} \approx 1$ mm geoid change

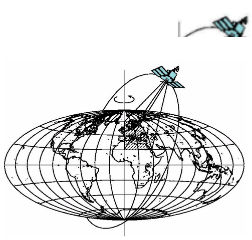

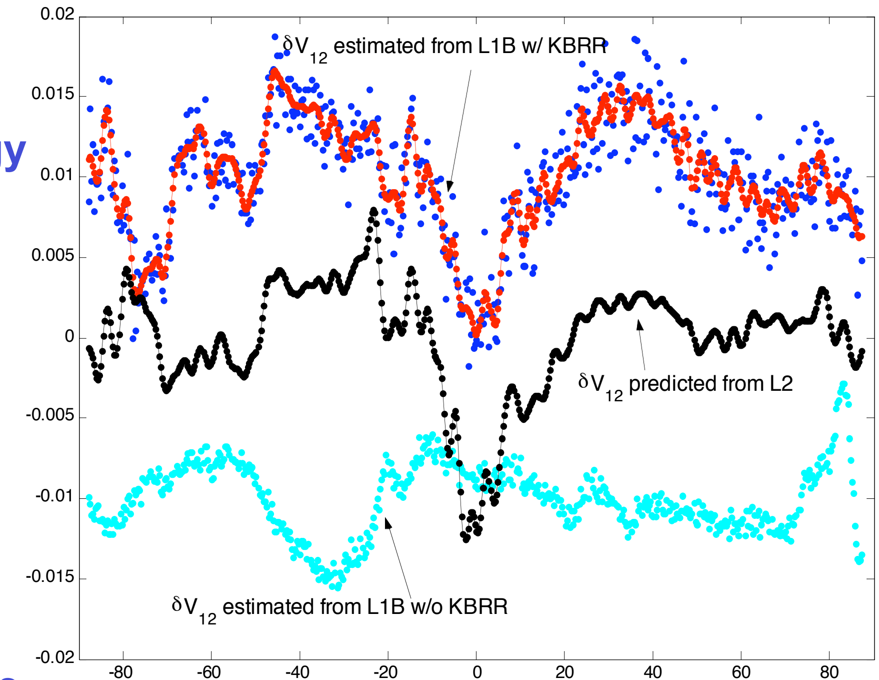

δV_{12} over Amazon basin versus latitude (GRACE descending pass)

School of Earth Sciences

Coseismic Deformation From GRACE
I. Regional solution

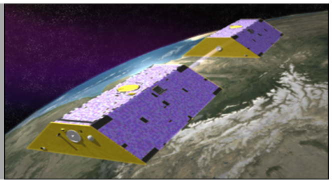

$$V_{12}^{hydrology}(r_1,\theta_1,\lambda_1,r_2,\theta_2,\lambda_2;t) = G\sum_{i=1}^{N\times M} m(\theta_i,\lambda_i,t)\left(\frac{1}{l_1^i}-\frac{1}{l_2^i}\right)$$

$l_1^i = \sqrt{R^2 + r_1^2 - 2Rr_1\cos\psi_1^i}$, $\cos\psi_1^i = \cos\theta_i\cos\theta_1 + \sin\theta_i\sin\theta_1\cos(\lambda_i-\lambda_1)$, r_1 θ_1 λ_1 : position of satellite 1

$l_2^i = \sqrt{R^2 + r_2^2 - 2Rr_2\cos\psi_2^i}$, $\cos\psi_2^i = \cos\theta_i\cos\theta_2 + \sin\theta_i\sin\theta_2\cos(\lambda_i-\lambda_2)$ r_2 θ_2 λ_2 : position of satellite 2

Coseismic deformation from GRACE

II. Spatio-spectral Localization Using Slepian Basis Function

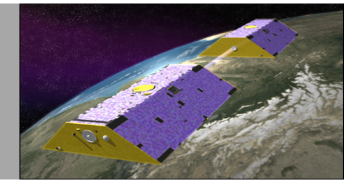

The Slepian functions are a family of band-limited spherical harmonic expansions that have the majority of their energy in the space domain concentrated within an arbitrary region on the unit sphere.

$$f(\hat{\mathbf{r}}) = \sum_{l=0}^{\infty} \sum_{m=-l}^{l} f_{lm} Y_{lm}(\hat{\mathbf{r}}), \qquad f_{lm} = \int_{\Omega} f \, Y_{lm} \, d\Omega, \quad \text{and} \quad \int_{\Omega} Y_{lm} Y_{l'm'} \, d\Omega = \delta_{ll'} \delta_{mm'}. \tag{1}$$

The Slepian basis for the domain R is the collection of bandlimited functions

$$g(\hat{\mathbf{r}}) = \sum_{l=0}^{L} \sum_{m=-l}^{l} g_{lm} Y_{lm}(\hat{\mathbf{r}}) \qquad \text{for which} \qquad \lambda = \int_{R} g^2(\hat{\mathbf{r}}) \, d\Omega \Big/ \int_{\Omega} g^2(\hat{\mathbf{r}}) \, d\Omega = \text{maximum}. \tag{2}$$

Maximizing equation (2) leads to the spectral-domain Hermitian, positive-definite eigenvalue equation

$$\sum_{l'=0}^{L} \sum_{m'=-l'}^{l'} D_{lm,l'm'} g_{l'm'} = \lambda g_{lm}, \quad \text{with} \quad D_{lm,l'm'} = \int_{R} Y_{lm} Y_{l'm'} \, d\Omega, \qquad 0 \le l \le L, \tag{3}$$

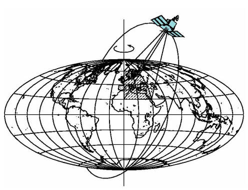

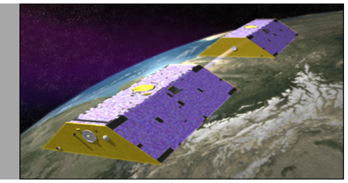

Coseismic deformation from GRACE

II. Spatio-spectral Localization Using Slepian Basis Function

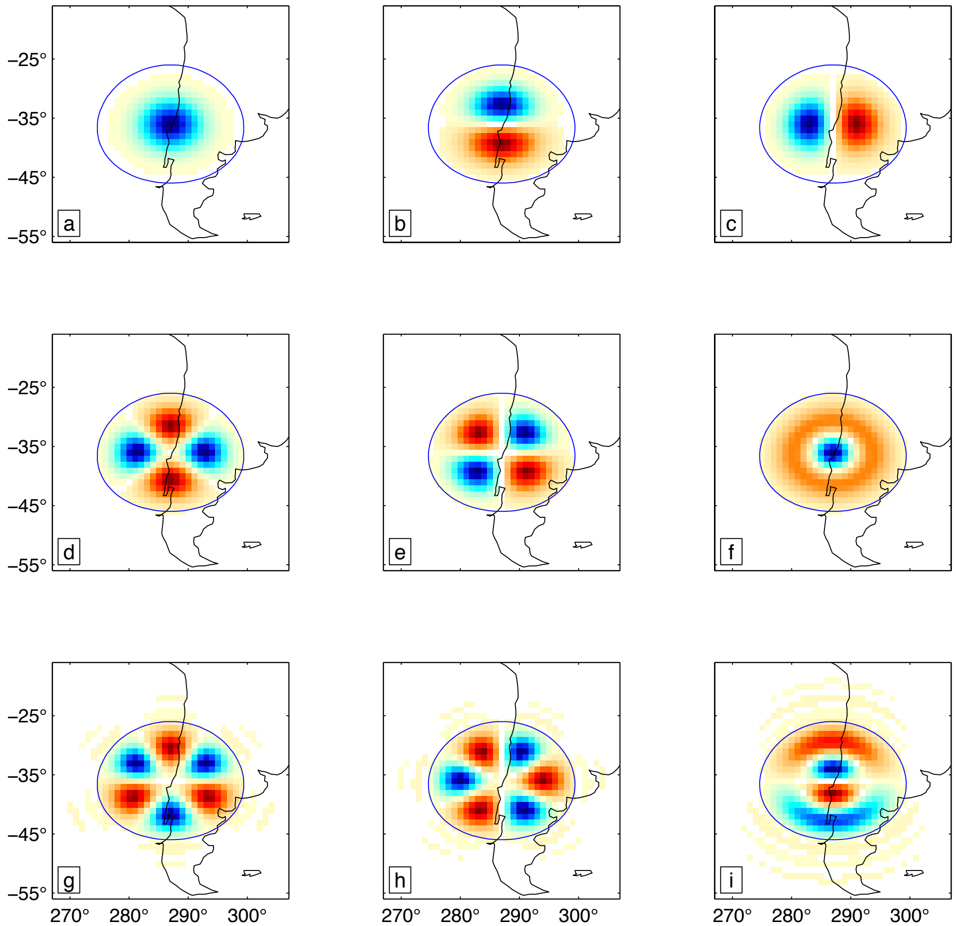

The first 9 bandlimited (maximum degree $L = 60$) Slepian basis functions for the circularly symmetric region with a radius $\phi = 10^{\mathrm{o}}$ centered on the epicenter of the 2010 offshore Maule earthquake.

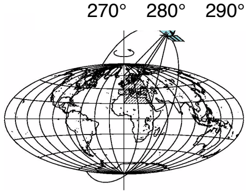

Coseismic deformation from GRACE

II. Spatio-spectral Localization Using Slepian Basis Function

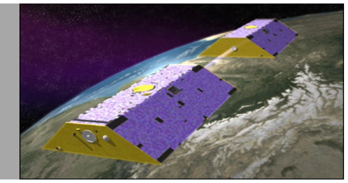

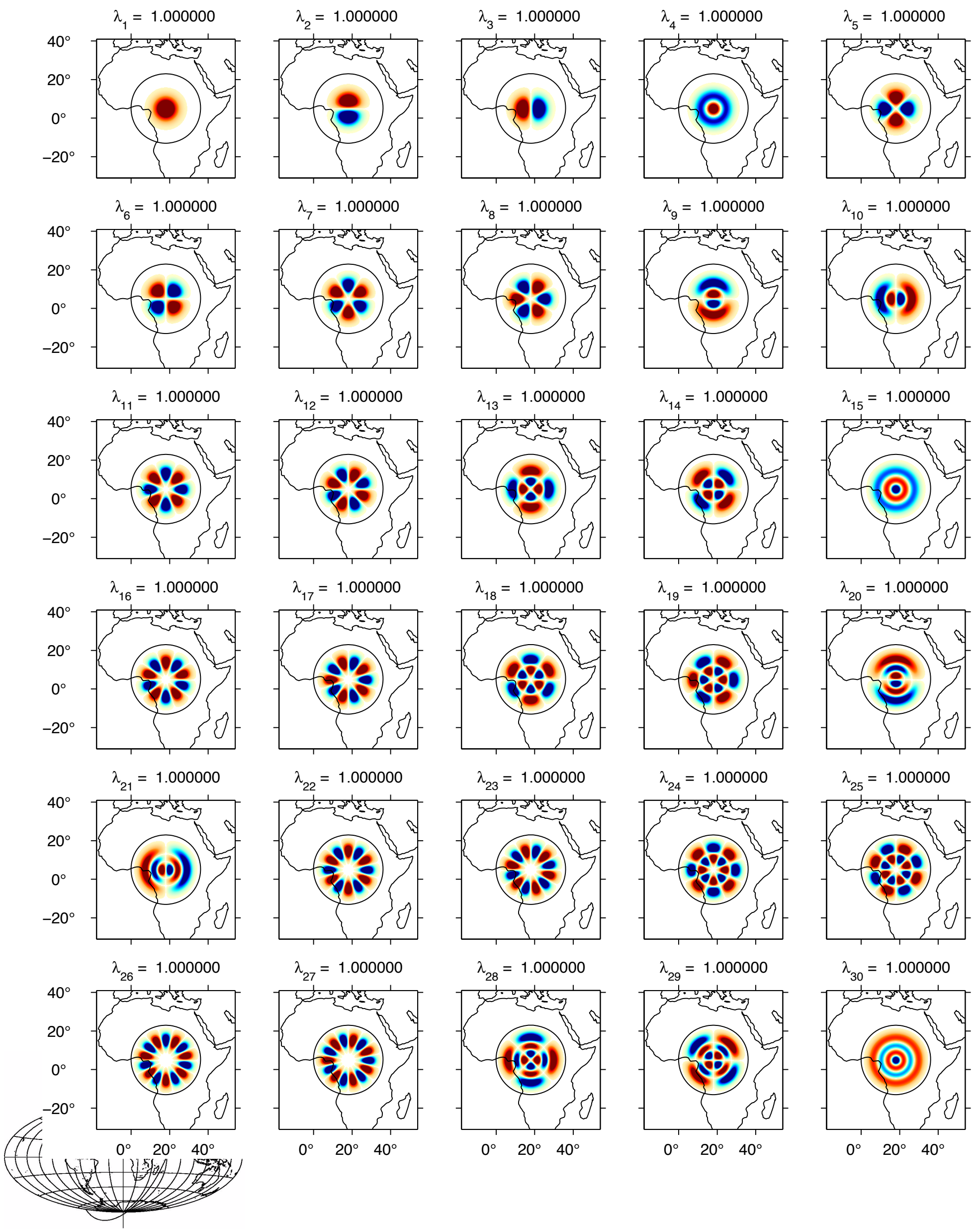

Another Example:

Optimally localized Slepian functions concentrated within a circularly symmetric domain of colatitudinal radius $\phi = 18^{o}$. The bandwidth is L=72 and the rounded Shannon number N = 30.

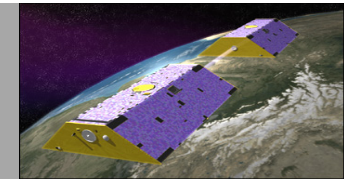

‘Sparsity’ by using Slepian analysis

When the signal of interest is spatially localized, and the Slepian basis designed to be concentrated inside of the same target region, the signal can be very well approximated by a truncated Slepian expansion limited to the first N, the Shannon number, terms:

$$s(\mathbf{r}) = \sum_{l=0}^{L} \sum_{m=-l}^{l} s_{lm} Y_{lm}(\mathbf{r}) = \sum_{\alpha=1}^{(L+1)^2} s_\alpha g_\alpha(\mathbf{r}) \approx \sum_{\alpha=1}^{N} s_\alpha g_\alpha(\mathbf{r}),$$

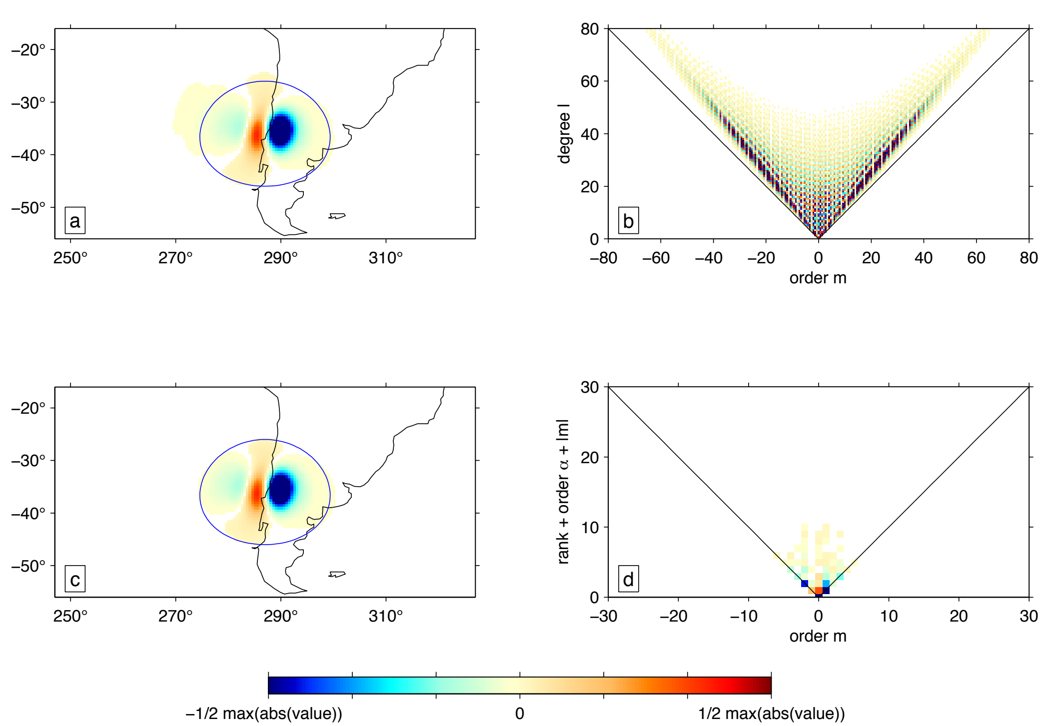

The sparsity that results from expanding localized geophysical signals in a Slepian basis. (a) Model-predicted coseismic gravity changes, band-limited to spherical harmonic degree and order 100 and (b) the corresponding ***10,201*** spherical harmonic expansion coefficients. (c) An approximation of the same signal using the ***N = 77*** best-localized Slepian functions concentrated to a circular region centered at the epicenter with radius of 10°, and (d) their Slepian expansion coefficients, using the same color scheme.

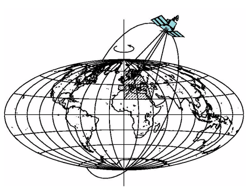

‘Sparsity’ by using Slepian analysis

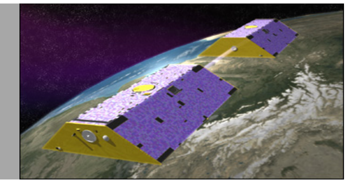

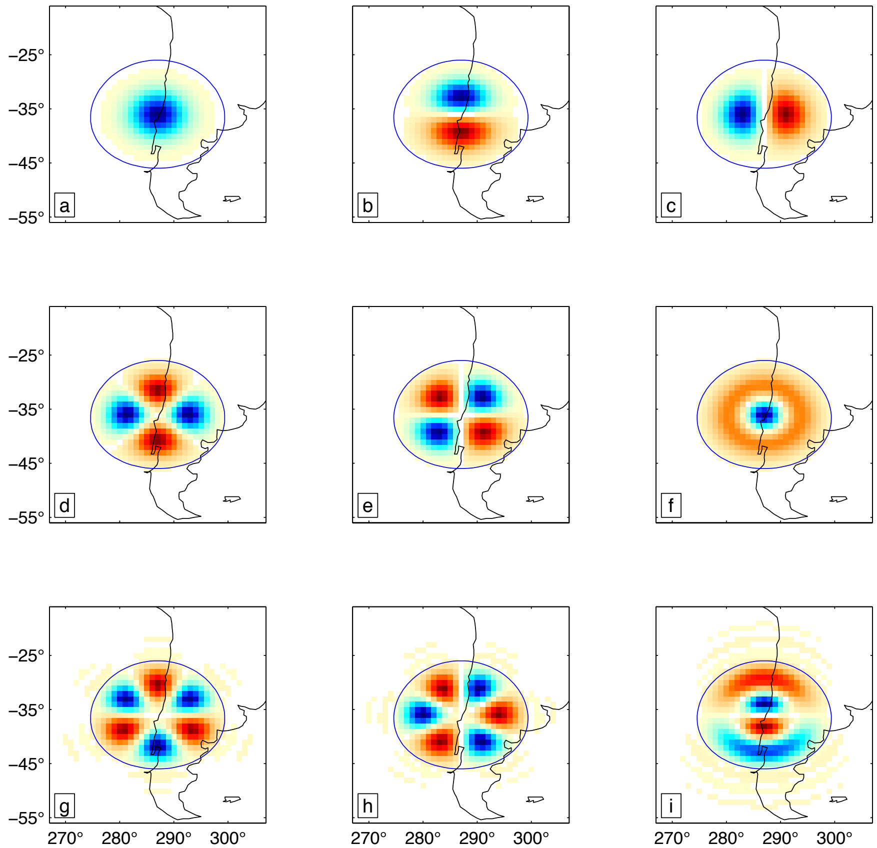

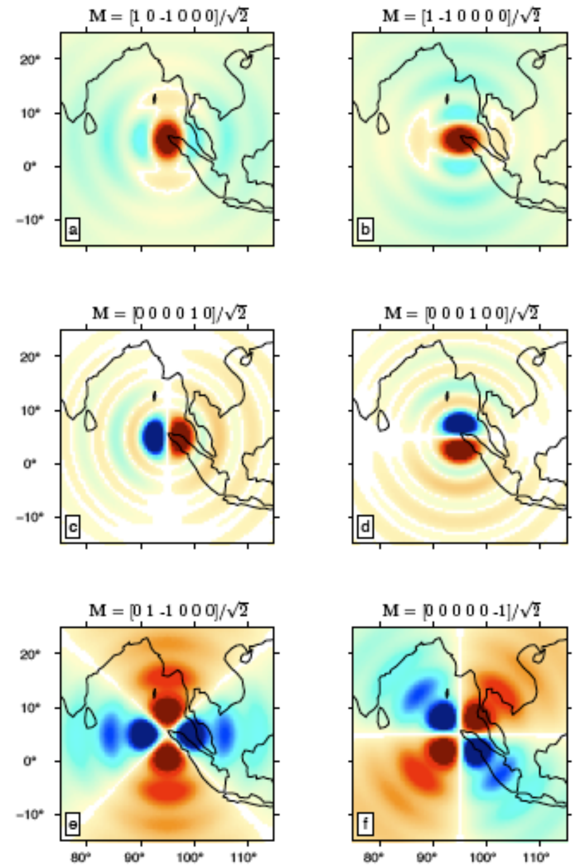

The top-ranked Slepian basis functions on circular concentration regions, fortuitously, match the patterns themselves of the geopotential perturbation generated by coseismic deformation. Using normal-mode theory, the first-order Eulerian gravitational potential perturbations in a spherically-symmetric non-rotating Earth due to a variety of earthquake focal-mechanism end-members corresponding to monopole, dipole, and quadrupole sources, form patterns that are similar to the shape of some of the best-concentrated Slepian functions on symmetric spherical caps

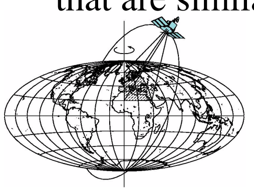

Tectonic Setting of Tohoku-Oki Earthquake

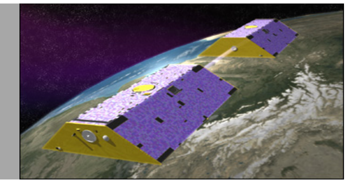

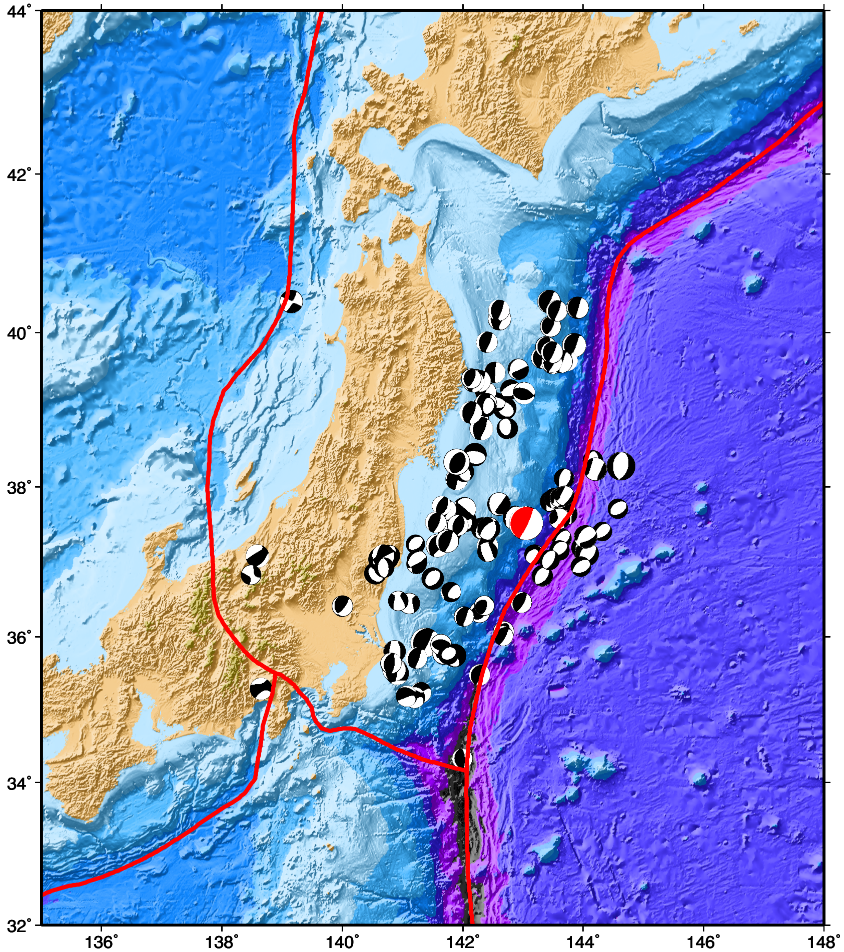

Occurred at plate boundary off Miyagi prefecture

Focal region from distribution of aftershocks:
Length : ~ 500km ; Width : ~ 200km

Thrust faulting on the subduction zone plate boundary between the Pacific and North America plates

Sea Floor Geodetic Observation

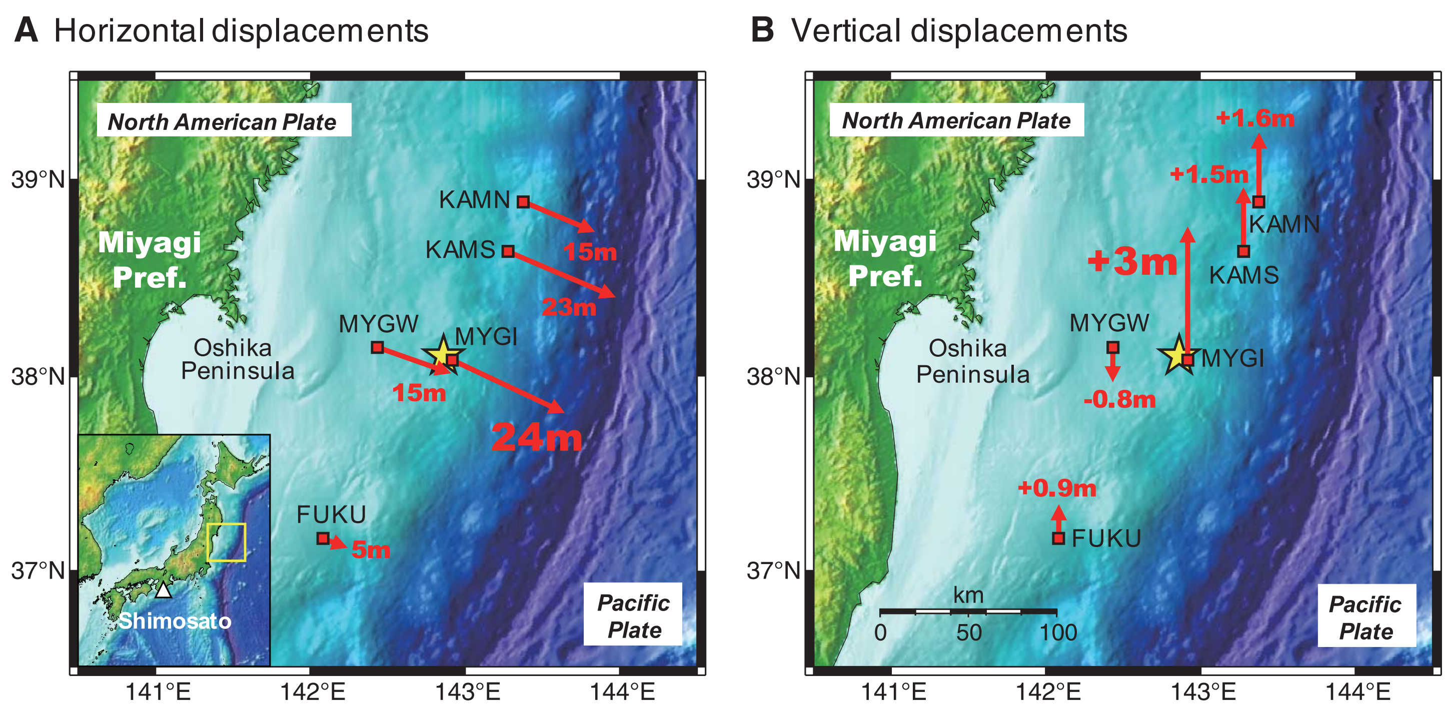

Fig. 1. Horizontal (**A**) and vertical (**B**) coseismic displacements at the sea-floor reference points, associated with the 2011 Tohoku-Oki earthquake. Red squares and a yellow star show locations of sea-floor reference points and the epicenter, respectively. The position reference is Shimosato (an open triangle).

[Sato et al., 2011]

Displacement Prediction vs. Geodetic Observation ------ USGS Model

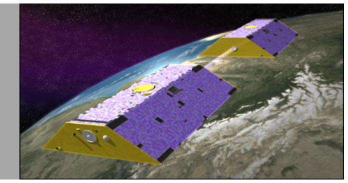

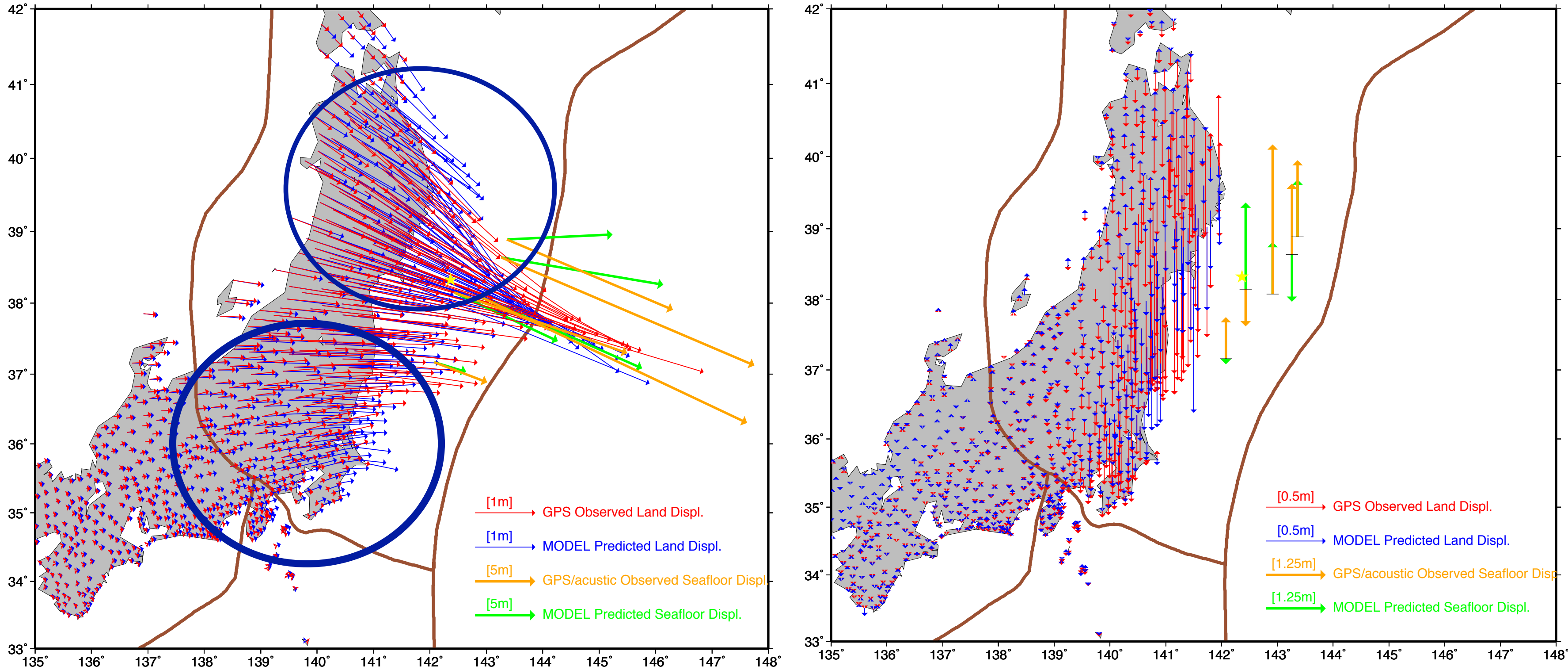

39 teleseismic broadband P waveforms, 22 broadband SH waveforms, and 55 long period surface waves

Displacement Prediction vs. Geodetic Observation ------ Caltech Model

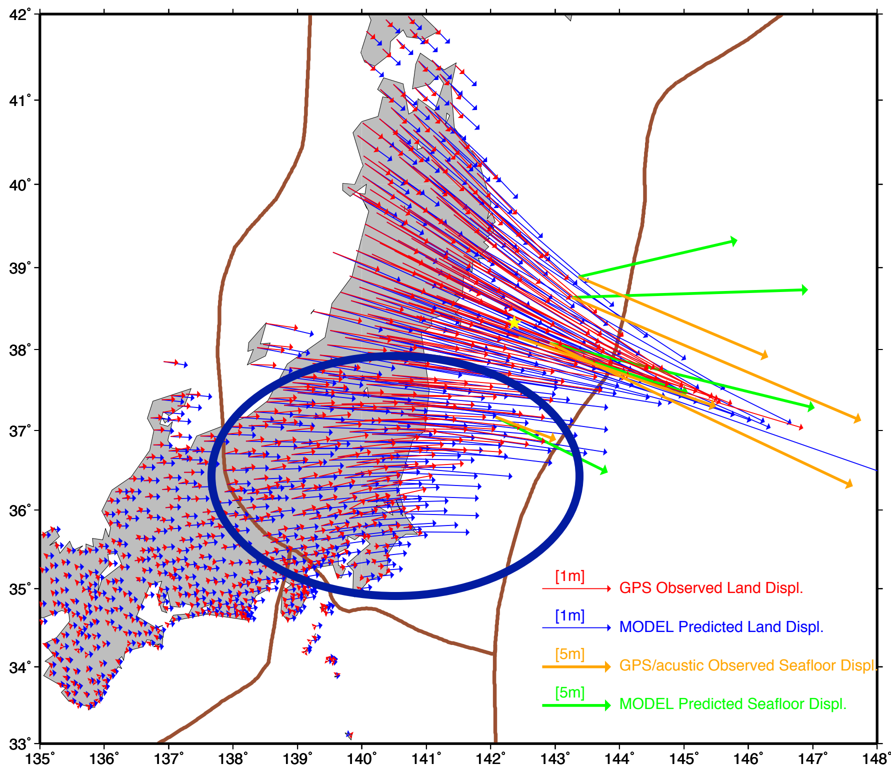

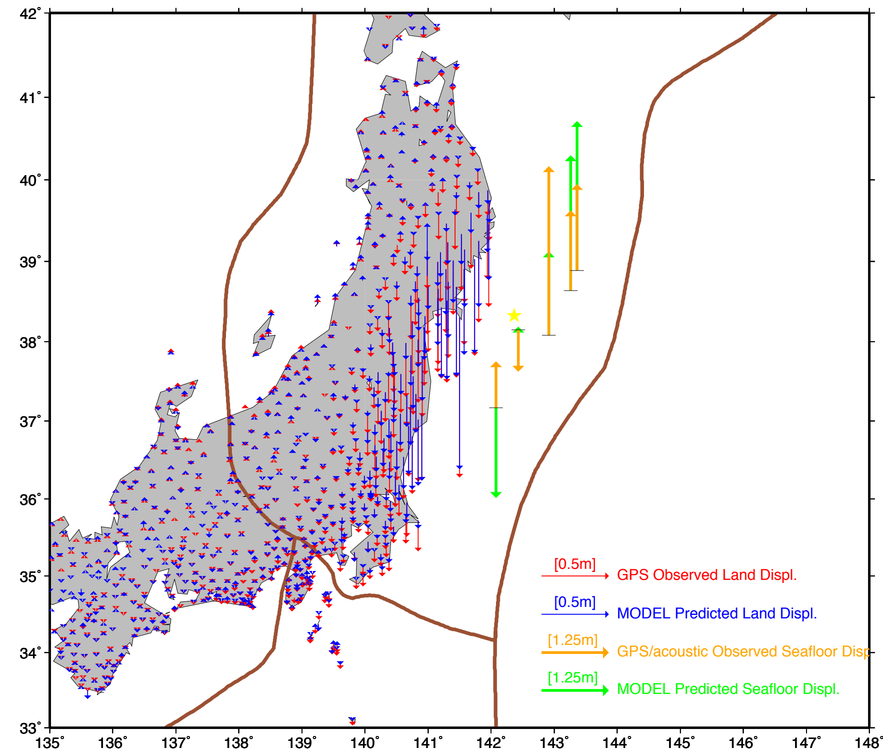

GPS data: preliminary solution (version 1.0) provided by the ARIA team at JPL and Caltech.

Seismic data: 27 teleseismic P waveforms and 21 SH waveforms

Displacement Prediction vs. Geodetic Observation
------ UCSB Model [Chenji et al.]

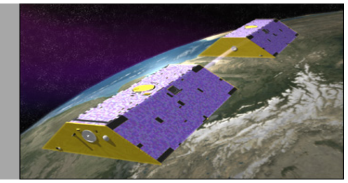

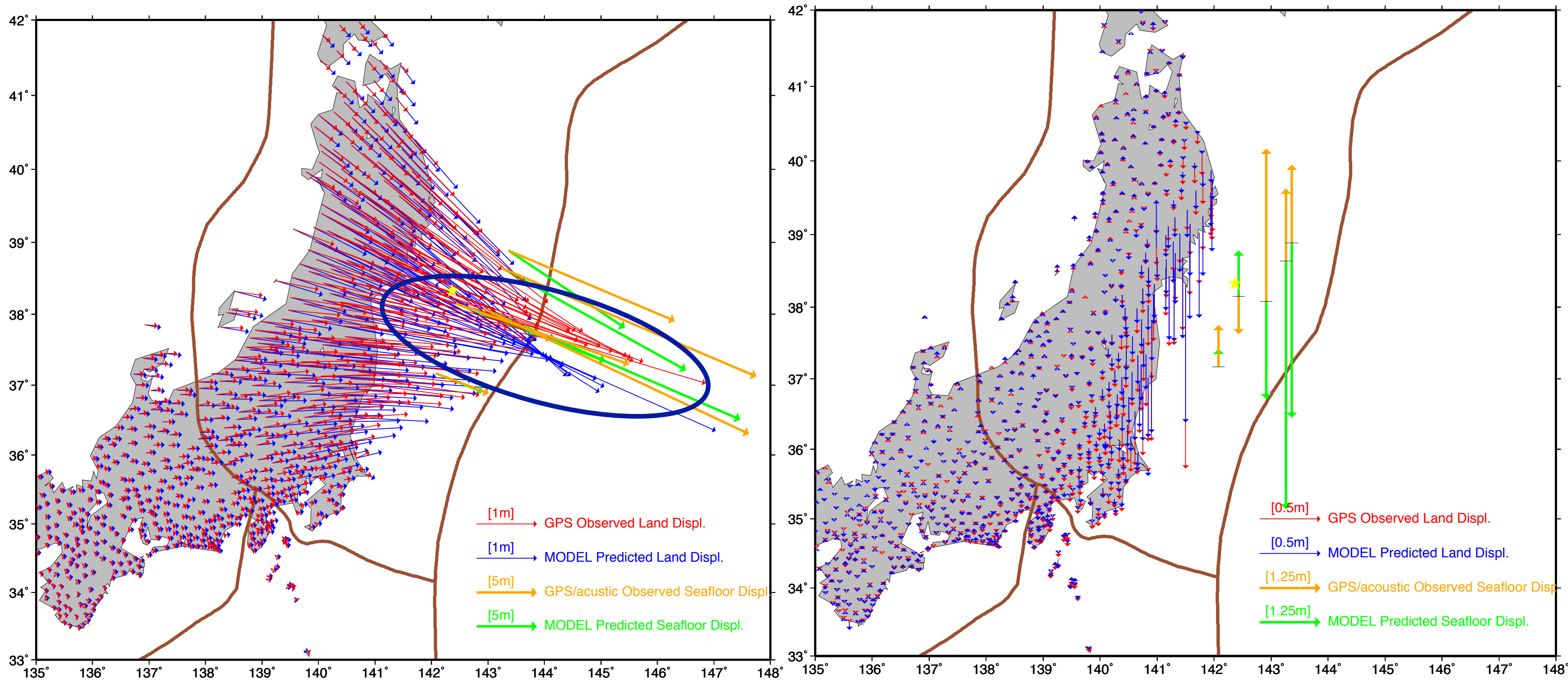

28 teleseismic broadband P waveforms, 25 broadband SH waveforms, and 54 long period surface waves

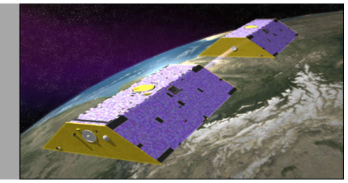

Assuming homogenous half-space: (Okada 1992)

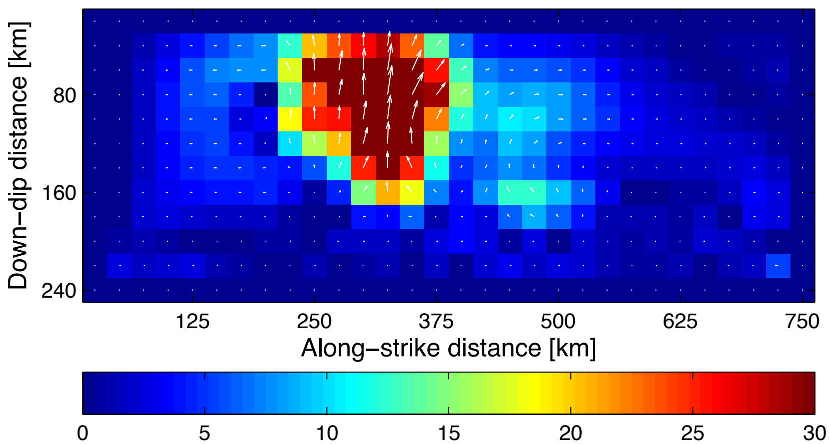

Model I:
Slip model inversion
with seafloor
geodetic observation

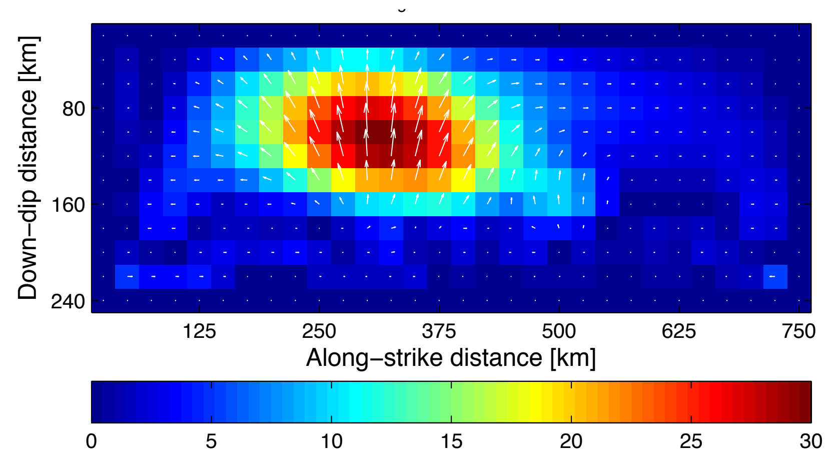

Model II:
Slip model inversion
using GPS only

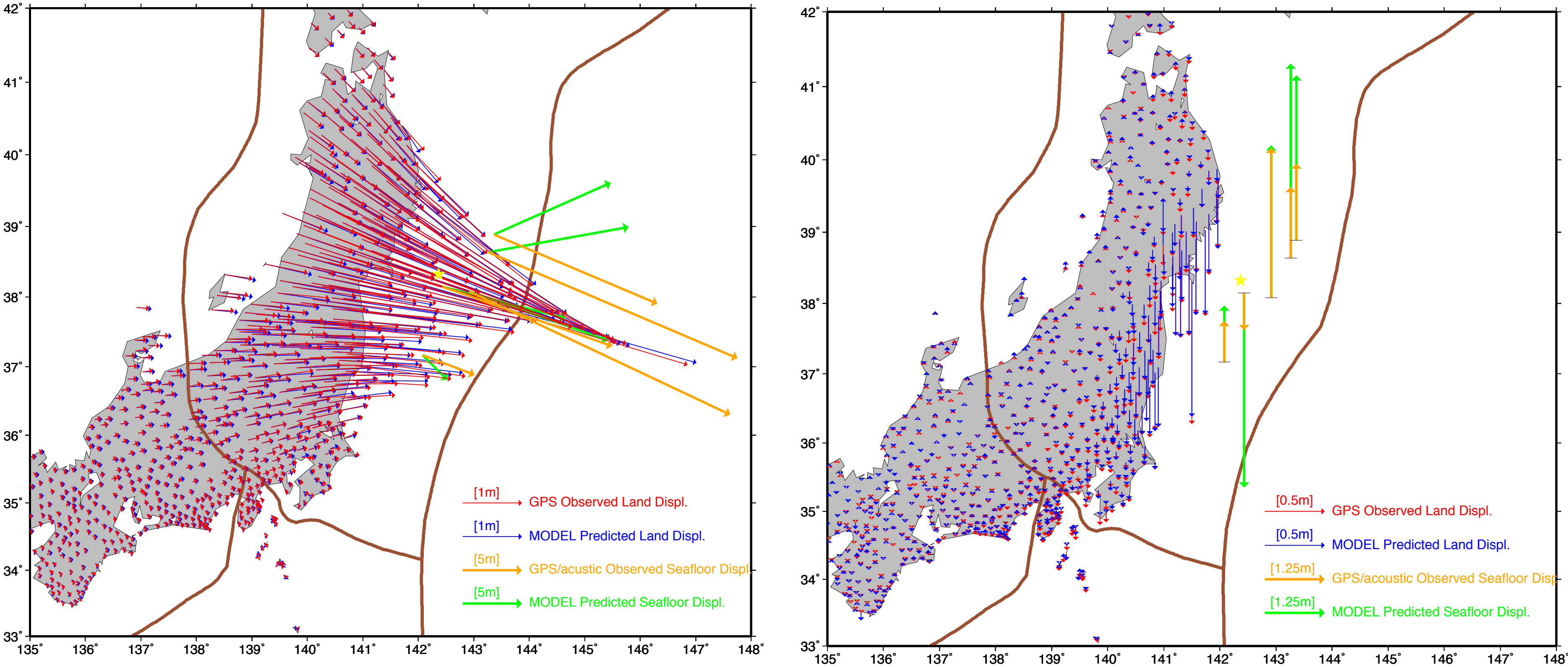

Coseismic displacement predicted by the inverted slip model using only GPS observation

School of Earth Sciences

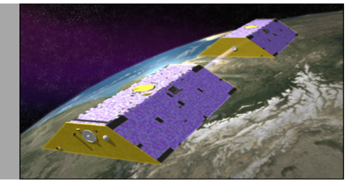

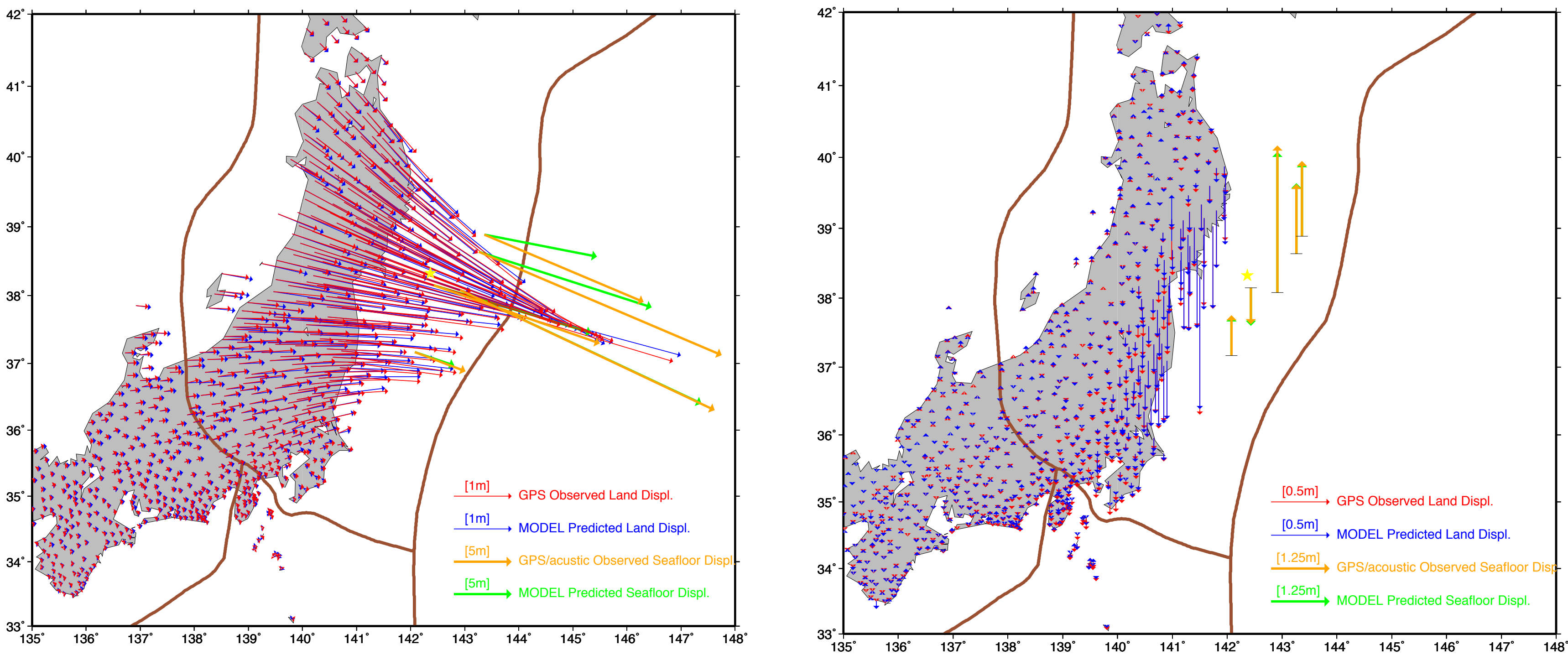

Coseismic displacement predicted by the inverted slip model using both GPS observation and Sea floor geodetic measurement

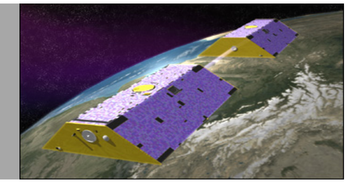

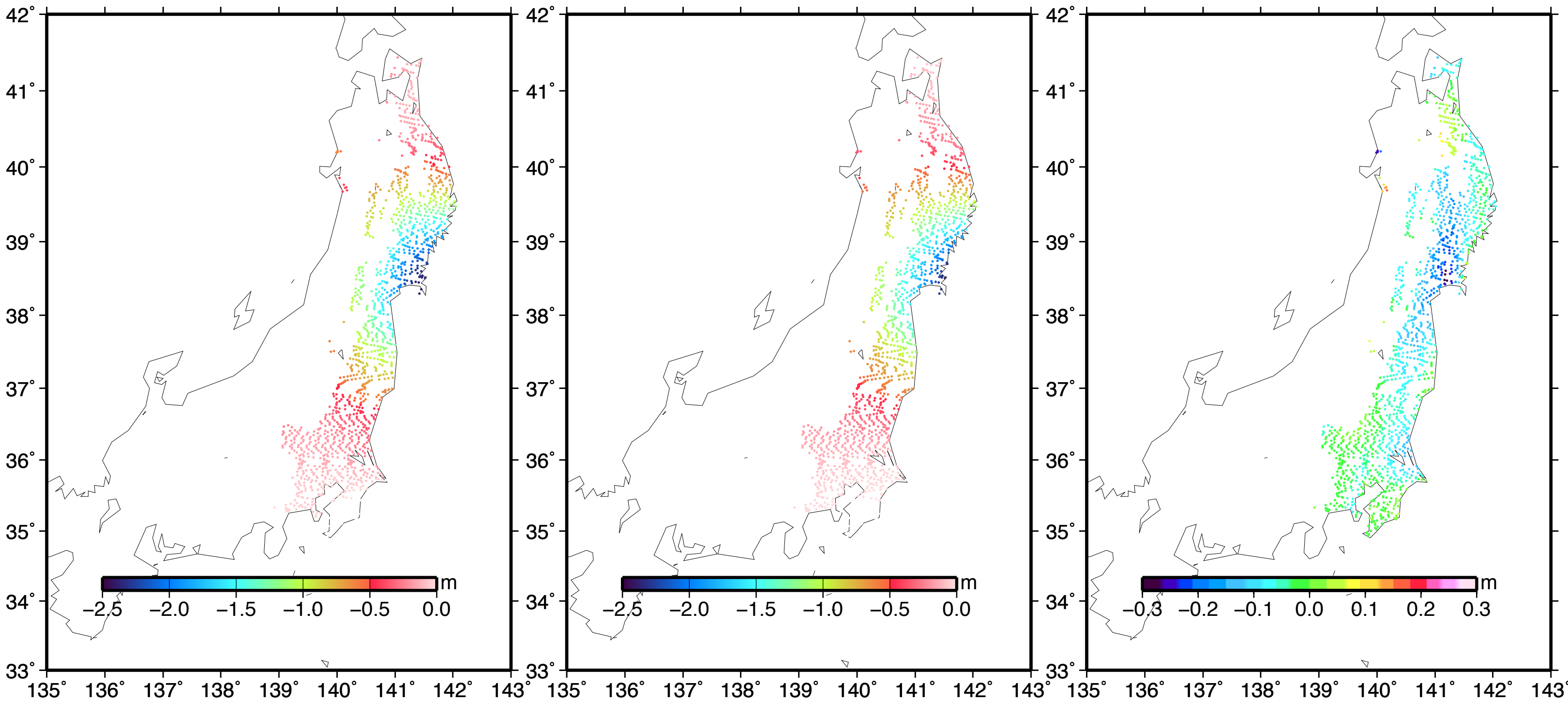

Asar observed LOS displacement

Model predicted LOS displacement

Observation – model prediction

THE OHIO STATE UNIVERSITY

School of Earth Sciences

Example II: localization analysis for Sumatra Earthquake

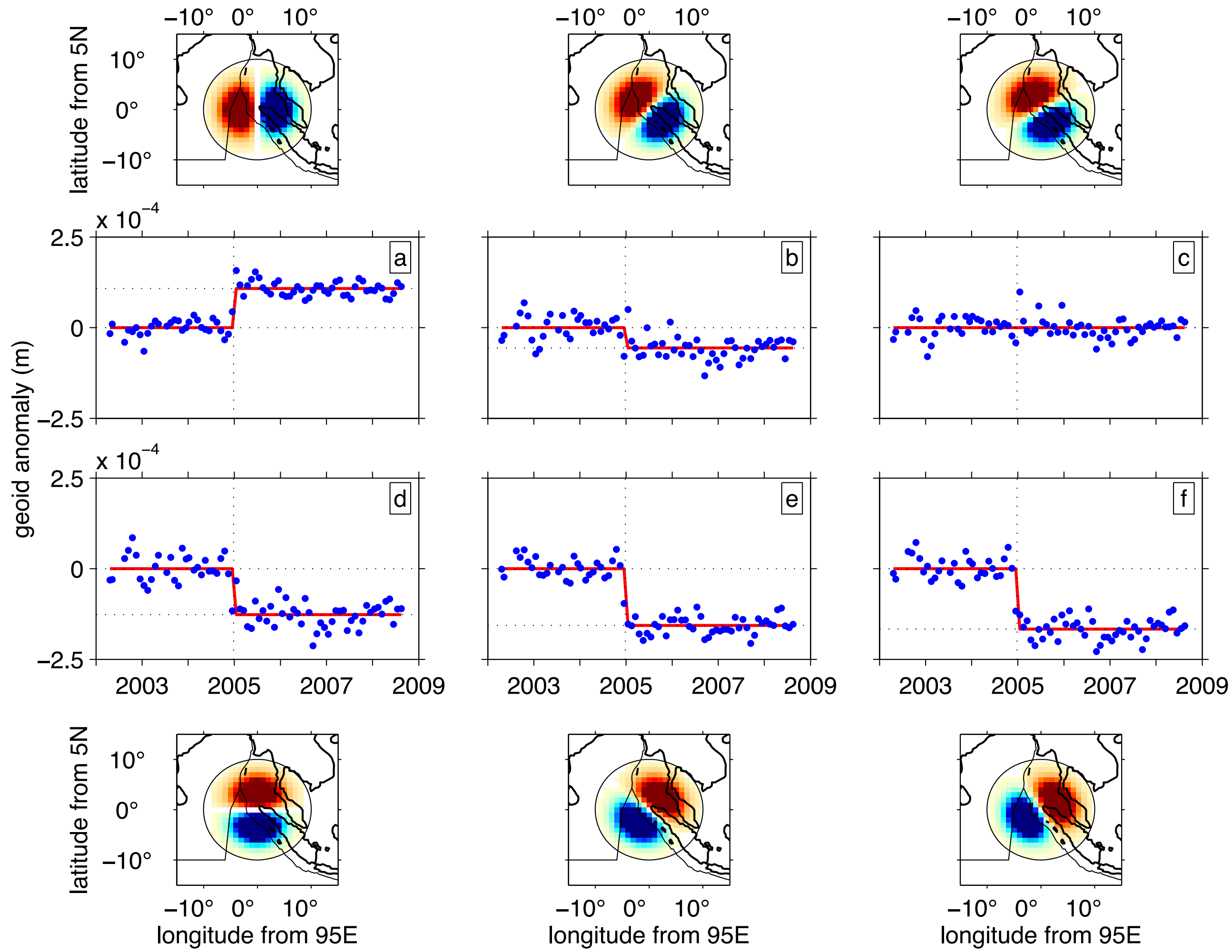

Example III: localization analysis for Maule Chile Earthquake

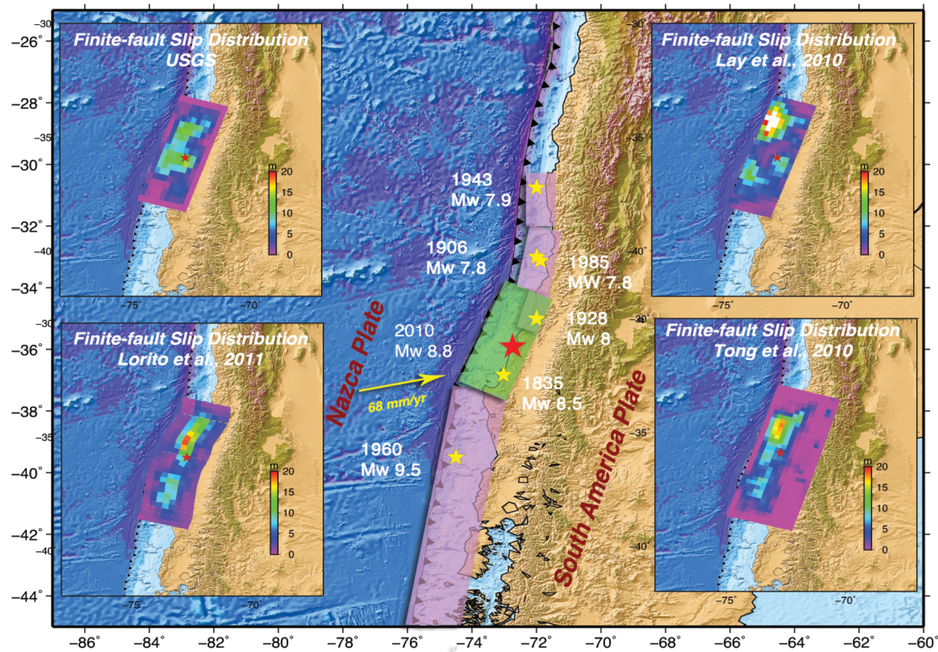

Maule earthquake ruptured over 500 km along a mature seismic gap between 34ºS and 38ºS – the Concepción-Constitución gap, where no large megathrust earthquakes had occurred since the 1835 Mw ~8.5 event.

	Publisher	Fault plane length	Fault plane width	Dimension of patches	strike	dip	Top edge depth	Data source
MODEL I	UCSB/USGS, Chen Ji	540km	200km	18x10	17.5º	18º	2.9km	Tele-seismic waves
MODEL II	Lay et al. 2010	575km	180km	23x9	18º	18º	4km	Tele-seismic waves (P&SH)
MODEL III	Tong et al. 2010	669.8 km	260km	34x13	16.8º	15º	2.6km	InSAR and GPS
MODEL IV	Lorito et al. 2011	625 km	200 km	25x8	2º~30º	10º~22º	9km	InSAR,GPS and tsunami

School of Earth Sciences

GRACE observation: 2010 Maule Earthquake

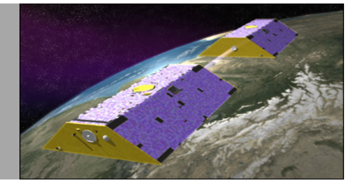

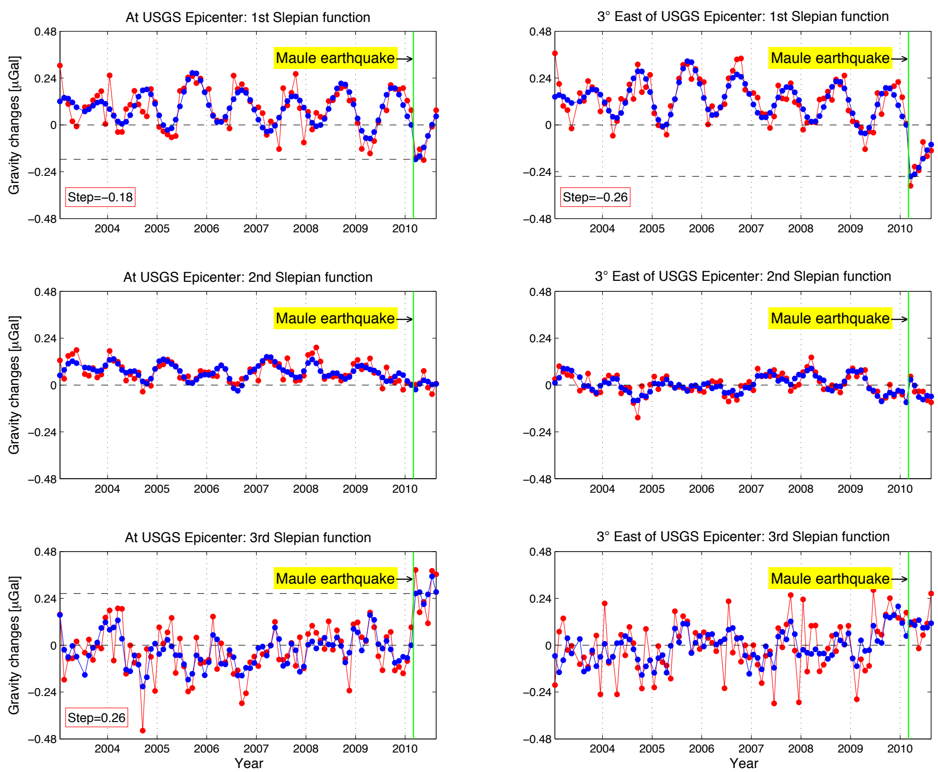

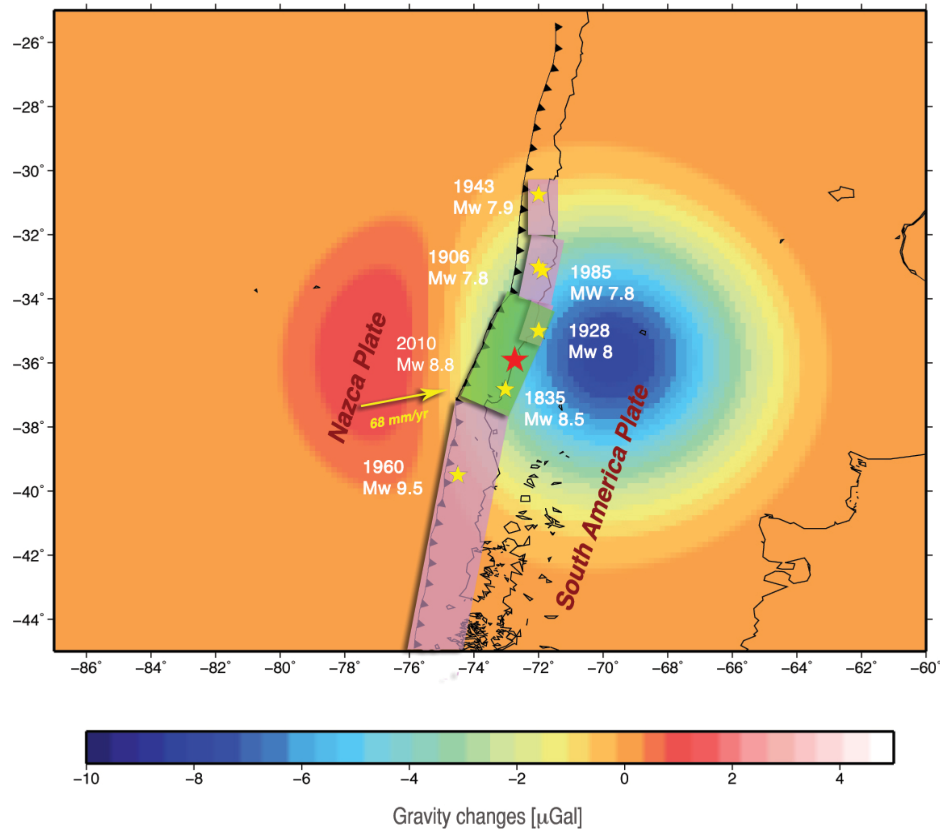

Time series of the Slepian coefficients
[CSR monthly gravity field production release 04]

GRACE detected coseismic gravity changes
Using Slepian analysis

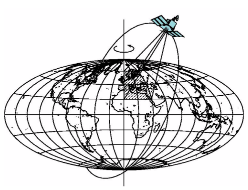

School of Earth Sciences

GRACE is sensitive to Chile earthquake, Ok… Then what …?

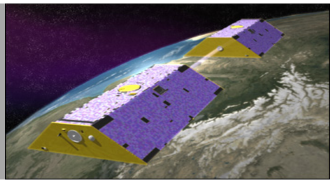

An example showing the sensitivity of gravity observation to faulting parameters

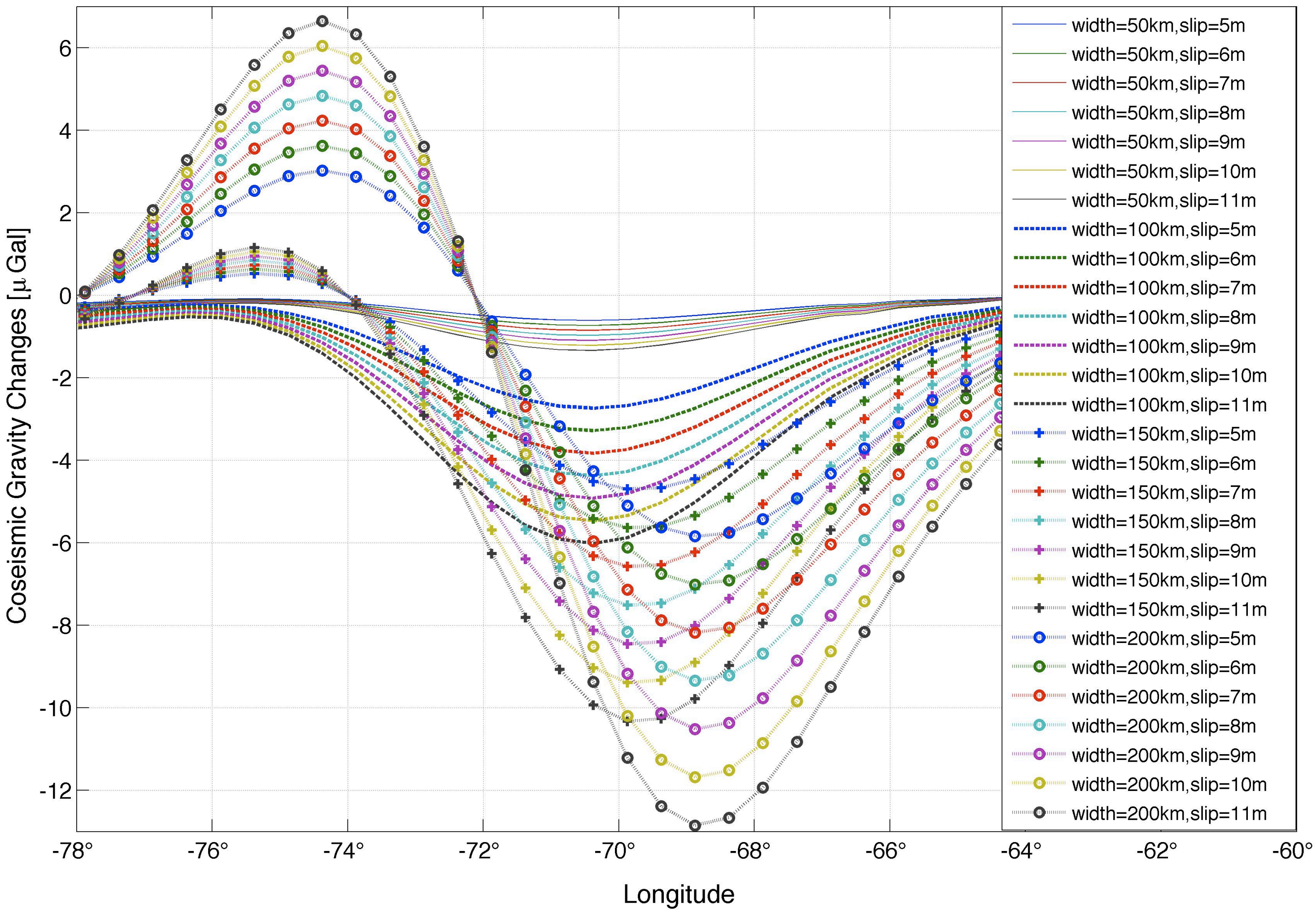

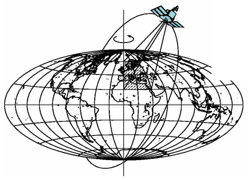

Independent constrains from GRACE for faulting mechanism

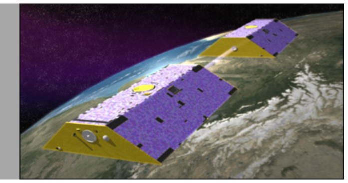

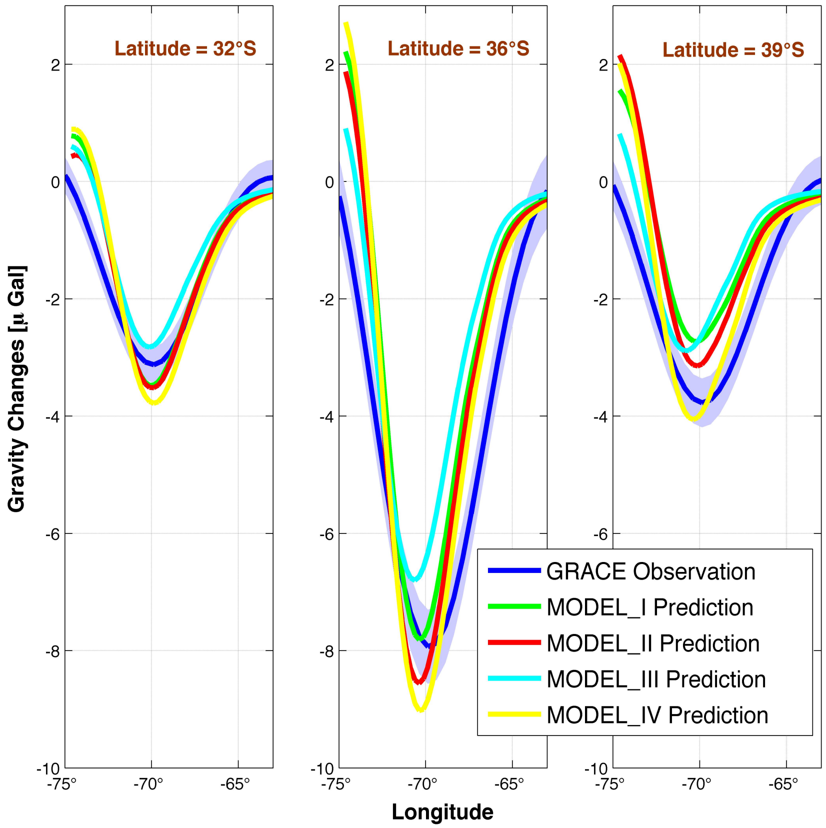

Comparison between observation & modelings of coseismic gravity changes

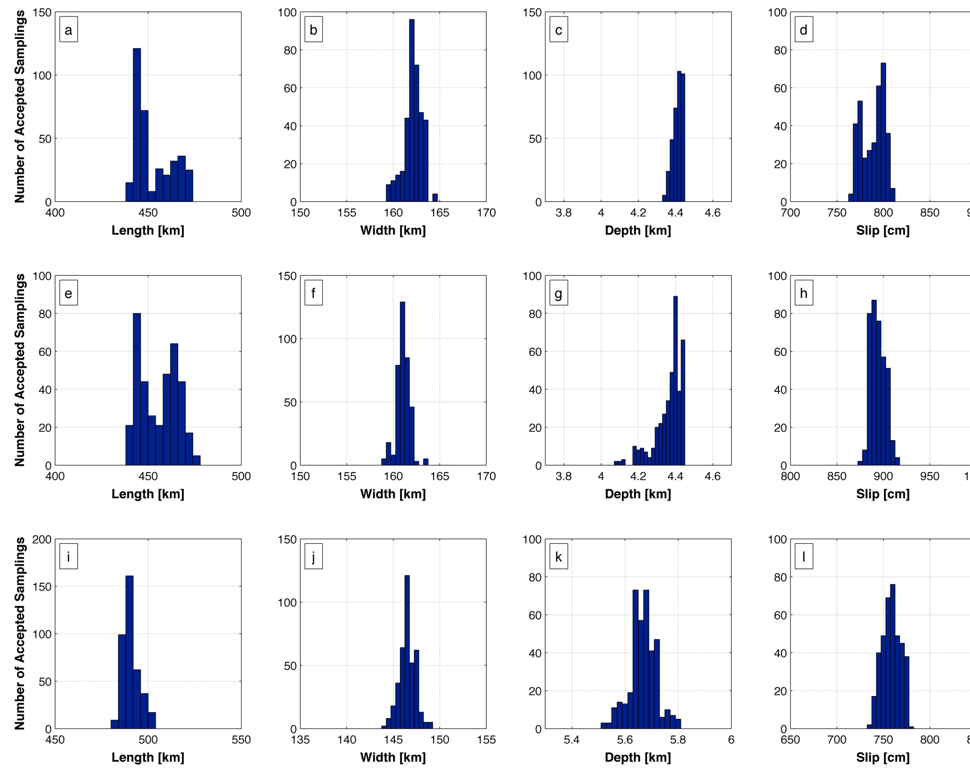

“Simulated annealing” - Independently invert faulting parameters from GRACE observation

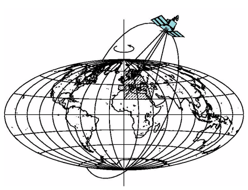

Independent constrains from GRACE for faulting mechanism

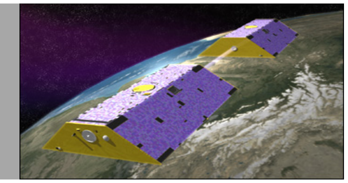

- estimated fault plane with length, width and depth of 445±40 km,162±20 km and 4.4±1.0 km, respectively, and an estimated uniform slip of 7.9±1.0 m. Assuming a mean rigidity of 30 GPa, the GRACE-derived new total seismic moment is 1.72×10^{22} Nm, resulting in Mw8.8, which is comparable to contemporary solutions

- if we assume the plate interface in Concepción-Constitución gap had remained fully locked for 175 years between 1835 and 2010, considering the plate convergence rate of 62～68 mm/yr, the slip is expected to be 11~12 m if the stresses accumulated in the Constitución gap were completely released during the 2010 Maule event. The slip deficit between the GRACE estimate (7.9±1.0 m) and the full-plate-coupling expectation implies incomplete moment release. In other words, there should be still some unbroken coupling zones remain in Constitución gap.

Coseismic Gravity Gradients Observation and its Interpretation

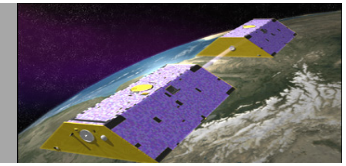

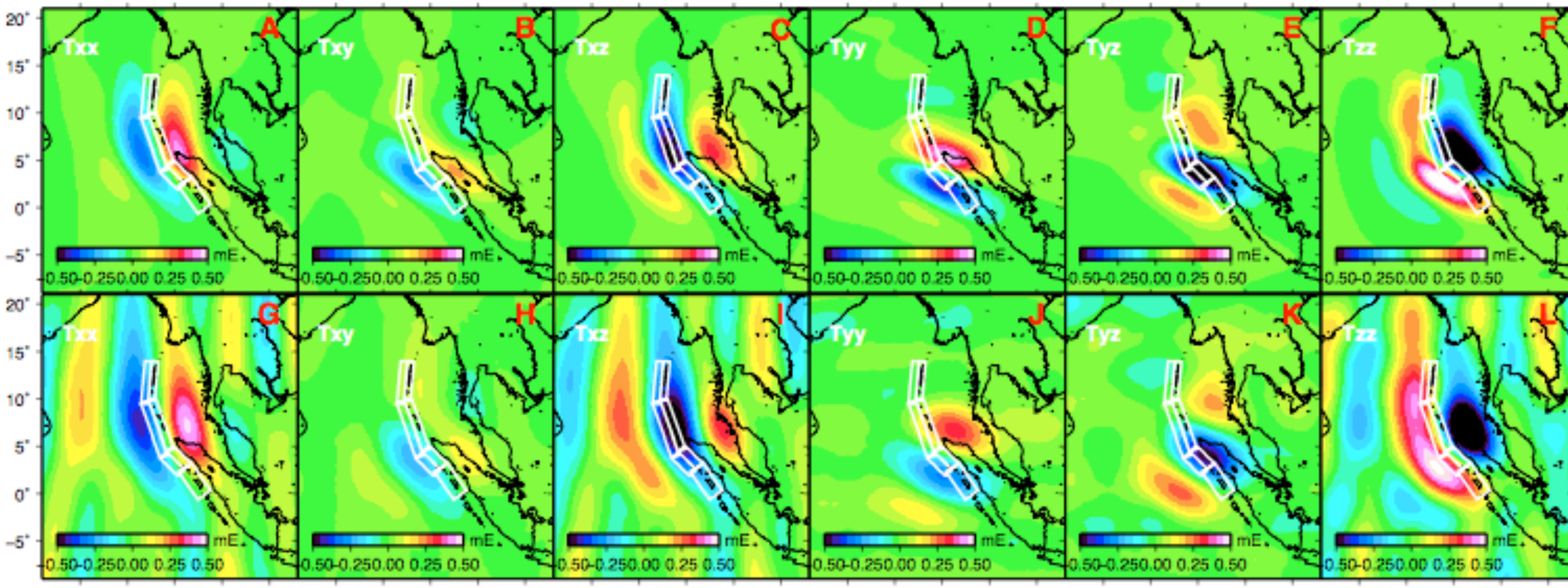

First row: Seismic model predicted total coseismic gravity gradients changes [in unit of miliEotvos], i.e., the summation of contribution from vertical displace on sea floor/Moho and from density change.
Second row: GRACE observed coseismic gravity gradients changes.

Why gravity gradients observation:

- Better delineate the faulting zone, and help indicate the edges of the fault plane
- More crust deformation then mantle deformation.
- Most valuable - Detailed slip distribution! which would greatly improve understanding about faulting mechanism, and help cease controversies among various models

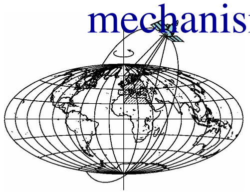

School of Earth Sciences